Journal of Computational Physics 492 (2023) 112414

Contents lists available at ScienceDirect

Journal of Computational Physics

journal homepage: www.elsevier.com/locate/jcp

# A family of structure-preserving exponential time differencing Runge–Kutta schemes for the viscous Cahn–Hilliard equation

Jingwei Sun, Hong Zhang*, Xu Qian, Songhe Song

*Department of Mathematics, National University of Defense Technology, Changsha 410073, PR China*

ARTICLE INFO

*Article history:*
Received 28 September 2022
Received in revised form 8 June 2023
Accepted 2 August 2023
Available online 9 August 2023

*Keywords:*
Viscous Cahn–Hilliard equation
Stabilized exponential time differencing scheme
Maximum principle
Energy stability
Mass conservation

ABSTRACT

We consider the numerical approximations of the viscous Cahn–Hilliard equation with either the Ginzburg–Landau polynomial potential or Flory–Huggins logarithmic potential. One challenge in solving such a fourth-order-in-space system is to develop accurate temporal discretization to preserve the energy stability, mass conservation, and maximum principle. We resolve this issue by developing a family of first- and second-order time marching schemes based on exponential time differencing Runge–Kutta (ETDRK) methods. We prove that the proposed schemes unconditionally preserve the three characteristics of the viscous Cahn–Hilliard equation. Because of the preservation of maximum principle, an error estimate in the infinity-norm is derived for the fully discrete system. Various numerical experiments are performed to verify the theoretical results and demonstrate the excellent performance of the proposed schemes.



## 1. Introduction

In this paper, we construct structure-preserving unconditionally stable schemes for the viscous Cahn–Hilliard equation

$$\begin{cases} \dfrac{\partial u}{\partial t} + \epsilon^2 \Delta^2 u - \Delta f(u) - \nu \Delta \dfrac{\partial u}{\partial t} = 0, \quad (\mathbf{x}, t) \in \Omega \times (0, T], \\ u|_{t=0} = u_0, \end{cases} \tag{1.1}$$

where $u$ is the order parameter, which varies continuously through the diffuse interface separating the pure states, $\Omega \subset \mathbb{R}^n$ $(n = 1, 2, 3)$ is a bounded domain, and $\epsilon \ll 1$ is the positive diffusion coefficient, which is related to the surface tension at the interface. Further, $f$ is the derivative of the chemical potential $F$, which is generally given by either the Ginzburg–Landau polynomial potential, i.e.,

$$F(u) = \frac{1}{4}(1 - u^2)^2, \quad f(u) = u^3 - u, \tag{1.2}$$

or the Flory–Huggins logarithmic potential, i.e.,

* Corresponding author.
*E-mail addresses:* sjw@nudt.edu.cn (J. Sun), zhanghnudt@163.com (H. Zhang), qianxu@nudt.edu.cn (X. Qian), shsong@nudt.edu.cn (S. Song).

https://doi.org/10.1016/j.jcp.2023.112414
0021-9991/

$$F(u) = \frac{\theta}{2}[(1+u)\ln(1+u) + (1-u)\ln(1-u)] - \frac{\theta_c}{2}u^2, \quad 0 < \theta < \theta_c,$$
$$f(u) = \frac{\theta}{2}\ln\frac{1+u}{1-u} - \theta_c u. \tag{1.3}$$

It should be noted that the condition $\theta < \theta_c$ ensures that $F$ has a double-well form and that phase separation can occur. The positive parameter $\nu$ in Eq. (1.1) represents the viscosity coefficient, and Eq. (1.1) will degrade to the Cahn–Hilliard equation if $\nu = 0$.

### 1.1. Preliminaries

The viscous Cahn–Hilliard equation was proposed by Novick-Cohen [1] to introduce additional regularity and certain viscous effects neglected in the Cahn–Hilliard equation [2], for describing the dynamics of phase transitions. In recent three decades, much literature aimed to research the mathematical analysis of the viscous Cahn–Hilliard equation, such as the well-posedness, long-time asymptotic behaviors, and global attractors (see, e.g. [3–10]). Among them, we are more concerned with the intrinsic properties which play a vital role in maintaining the long-time behavior and stability of the numerical solutions. Roughly speaking, for the viscous Cahn–Hilliard equation, the structure-preserving properties include the mass conservation law, the energy dissipation law, and the maximum principle. In what follows we describe these properties in detail.

(1) Mass conservation law.

Same as the Cahn–Hilliard equation, the viscous Cahn–Hilliard equation with (i) periodic boundary conditions on $\Omega = \prod_{i=1}^{d}(a_i, b_i)$,

$$\frac{\partial^j u}{\partial x_i^j}|_{x_i=a_i} = \frac{\partial^j u}{\partial x_i^j}|_{x_i=b_i}, \quad i = 1, \cdots, d, \ j = 0, \cdots, 3,$$

or (ii) homogeneous Neumann boundary conditions

$$\mathbf{n}\cdot\nabla u = 0 \text{ and } \mathbf{n}\cdot\nabla[\epsilon^2\Delta u - f(u)] = 0, \quad \text{on } \partial\Omega, \ t > 0$$

possess the conservation of mass; that is,

$$\frac{\mathrm{d}M(u)}{\mathrm{d}t} = \frac{\mathrm{d}}{\mathrm{d}t}\int_\Omega u(\mathbf{x})\mathrm{d}\mathbf{x} = 0. \tag{1.4}$$

It is noted that one generally does not consider Dirichlet boundary conditions precisely because they do not yield the conservation of mass.

(2) Energy dissipation law.

The viscous Cahn–Hilliard equation (1.1) is related to the Ginzburg–Landau free energy functional:

$$E(u) = \int_\Omega \left(\frac{\epsilon^2}{2}|\nabla u(\mathbf{x})|^2 + F(u(\mathbf{x}))\right)\mathrm{d}\mathbf{x}, \tag{1.5}$$

where the notation $|\cdot|$ denotes the usual Euclidean norm. To obtain the energy dissipation law, let us define the gradient of $E(u)$ in a nonstandard Hilbert space $\mathcal{H} := \{u \in L^2(\Omega) | \int_\Omega u(\mathbf{x})\mathrm{d}\mathbf{x} = 0\}$. Let $\mathcal{I}$ be the identity operator, we introduce an invertible, self-adjoint operator $\mathcal{A} : u \to -(\mathcal{I} - \nu\Delta)^{-1}\Delta u$ [11,12] on $\mathcal{H}$ subject to periodic or homogeneous Neumann boundary conditions, where $(\mathcal{I} - \nu\Delta)^{-1}$ is defined by setting $v = (\mathcal{I} - \nu\Delta)^{-1}h$ when $v$ solves the problem

$$(\mathcal{I} - \nu\Delta)v = h, \quad x \in \Omega, \tag{1.6}$$

with the same boundary conditions.

We denote by $\langle\cdot,\cdot\rangle$ the usual $L^2$-inner product with associated norm $\|\cdot\|_2$, and set $\|\cdot\|_{-1} := \|(-\Delta)^{-\frac{1}{2}}\cdot\|_2$, where $(-\Delta)^{-1}$ is the inverse minus Laplace operator associated with prescribed boundary conditions and acting on $\mathcal{H}$. Since $\langle\mathcal{A}^{-1}u, v\rangle = \langle(-\Delta)^{-1}(\mathcal{I} - \nu\Delta)u, v\rangle = \langle(-\Delta)^{-1}u, v\rangle + \nu\langle u, v\rangle$ is a positive combination of inner products, the operator $\mathcal{A}^{-1}$ is positive definite. Then the $\mathcal{H}$ inner product and induced norm are respectively defined as

$$\langle u, v\rangle_{\mathcal{H}} := \langle\mathcal{A}^{-1}u, v\rangle, \quad \|u\|_{\mathcal{H}} := \langle u, u\rangle_{\mathcal{H}}^{\frac{1}{2}} = \sqrt{\|u\|_{-1}^2 + \nu\|u\|_2^2}.$$

The gradient of $E(u)$ on the space $\mathcal{H}$ is calculated as $\mathrm{grad}_{\mathcal{H}}E(u) = \mathcal{A}\frac{\delta E(u)}{\delta u}$, where $\frac{\delta}{\delta u}$ denotes the variational derivative. Finally, the $\mathcal{H}$-gradient flow for $E(u)$ gives rise to the viscous Cahn–Hilliard equation; that is,

$$\begin{aligned}\frac{\partial u}{\partial t} &= -\mathrm{grad}_{\mathcal{H}} E(u) = (\mathcal{I} - \nu\Delta)^{-1}\Delta[-\epsilon^2\Delta u + F'(u)] \\ &= (\mathcal{I} - \nu\Delta)^{-1}[-\epsilon^2\Delta^2 u + \Delta f(u)].\end{aligned} \tag{1.7}$$

Now we see that the total free energy $E(u)$ is decreasing in time,

$$\frac{\mathrm{d}E(u)}{\mathrm{d}t} = \left\langle \mathrm{grad}_{\mathcal{H}} E(u), \frac{\partial u}{\partial t} \right\rangle_{\mathcal{H}} = -\left\| \frac{\partial u}{\partial t} \right\|_{\mathcal{H}}^2 \leq 0. \tag{1.8}$$

(3) Maximum principle.

Besides the above two properties, the viscous Cahn–Hilliard equation (1.1) also admits the maximum bound principle in Ref. [13], which means that the absolute value of its solution is pointwisely bounded for all time by some specific constant under appropriate initial/boundary conditions. The maximum principle describes the stability in the sense of the $L^\infty$-norm. If the corresponding semi-discrete maximum principle is guaranteed, the numerical energy stability and convergence of the solution can be more easily analyzed [14]. By assuming that a general class of (singular) non-linearities $f \in C^1(-1, 1)$ (e.g., the Flory–Huggins logarithmic potential) satisfying

- $\lim_{u\to\pm 1} f(u) = \pm\infty$;
- $\lim_{u\to\pm 1} f'(u) = +\infty$,

Miranville and Zelik [15] analyzed and proved the strict separation property via the comparison principle and a priori estimate for the viscous Cahn–Hilliard equation (1.8); that is,

$$\|u(t)\|_{L^\infty(\Omega)} \leq 1 - \delta_{\mu,\epsilon,\nu}, \quad \forall t \geq \mu, \quad 0 < \delta_{\mu,\epsilon,\nu} < 1,$$

where the distance $\delta_{\mu,\epsilon,\nu}$ depends on the viscosity coefficient $\nu$, diffusion coefficient $\epsilon$, and time $\mu$ for a given potential.

### 1.2. Related work

Various studies have been devoted to the construction of efficient and accurate numerical methods that preserve the mass conservation and energy dissipation laws at the discrete level for certain gradient flows including the viscous Cahn–Hilliard equation. For spatial discretization, a partial list includes studies on the finite element method [16–18], finite difference method [19–21], and spectral method [22–25]. For temporal discretization, the backward Euler method was applied by Injrou et al. [26] to construct an unconditionally stable first-order scheme. A second-order fast explicit operator splitting method was constructed by Weng et al. [22] to enhance the accuracy and efficiency of computations. The invariant energy quadratization (IEQ) approach [27] and the scalar auxiliary variable (SAV) approach [23,28] were used to develop linearly implicit and unconditionally energy stable schemes for the viscous Cahn–Hilliard equation. Also, a series of second- and third-order energy stable backward differentiation formula (BDF) schemes were developed for the viscous Cahn–Hilliard equation and other phase-field models, see, e.g. [17,29–33].

In addition, the preservation of the numerical solution's boundedness is as important as the first two properties for constructing an accurate and robust numerical scheme. For instance, because of its favorable characteristics (energy dissipation law, maximum principle, and solution regularity), the Allen–Cahn equation is often used to develop various structure-preserving schemes in recent years, especially for the maximum-principle-preserving (MPP) aspect, such as implicit–explicit (IMEX) [34] and stabilized semi-implicit (SSI) approaches [35], Strang splitting method [36], Crank–Nicolson finite difference method [37], as well as the integrating factor type methods, see, e.g. [38–43]. The positivity-preserving methods of the Cahn–Hilliard equation with the Flory–Huggins logarithmic potential have also been extensively studied in previous research, see, e.g. [33,44–47,32]. The exponential time differencing (ETD) schemes come from the variation-of-constants formula with the nonlinear terms in the system approximated by polynomial interpolations, followed by exact integration of the resulted integrals. They were systemically investigated by Beylkin [48] and further developed for stiff systems by Cox and Matthews [49]. Extensive studies of ETDRK and ETD multi-step (ETDMS) schemes were carried out by Hochbruck and Ostermann [50,51]. In a series of papers, Du and Zhu [52,53] investigated the linear stabilities and applications of ETD schemes as well as their modifications. The research conducted by Wang and co-authors [54–56] involved the application of stabilized ETDMS schemes up to the third order for the molecular beam epitaxy (MBE) model by adding a third-order accurate Douglas-Dupont regularization term. Especially noteworthy is that in Ref [54], Wang et al. proved the discrete energy stability in a modified version via a careful Fourier eigenvalue analysis, and first derived a rigorous convergence estimate for a third-order accurate scheme for gradient flows. Du et al. [57] developed the unconditionally MPP ETD1 and ETDRK2 schemes for the nonlocal Allen–Cahn equation by utilizing a stabilization technique. Li et al. [58] and Jiang et al. [59] showed that these ETDRK schemes not only preserve the maximum principle unconditionally but also conserve the total mass for the mass-conservative Allen–Cahn equation. Huang et al. [60] also successfully applied the MPP ETD schemes to the Peng–Robinson equation of state, which is a widely used realistic equation of state for hydrocarbon fluids in the

petroleum industry. Given the many advantages and widespread applications of ETD methods, we study a family of ETDRK schemes, and prove that they unconditionally preserve the essential structure properties of the viscous Cahn–Hilliard equation, as shown in Section 3.

### 1.3. Outline of the paper

First, we briefly introduce the maximum principle derived by Zhang et al. [61] for the viscous Cahn–Hilliard equation in Section 2. In Section 3, we provide a family of stabilized ETDRK approaches and present detailed proofs that they can unconditionally preserve the energy dissipation, mass conservation and maximum principle for the viscous Cahn–Hilliard equation. After this, we study the error estimate of the proposed fully discrete schemes in Section 4 and present numerical results to support our theory and analysis in Section 5. Finally, we summarize our findings and present some directions for future research in Section 6.

## 2. Reformulation, stabilization and maximum principle for viscous Cahn–Hilliard equation

We first introduce a lemma which will be used to derive the maximum principle of the viscous Cahn–Hilliard equation.

**Lemma 2.1.** *[62] Let $h \in L^\infty(\Omega)$. Then, the problem (1.6) has a unique solution $v$ that lies in $W^{2,p}(\Omega)$ for all $p$, $1 < p < \infty$. If $h(\mathbf{x})$ is not constant almost everywhere, then*

$$\operatorname{ess\,inf} h(\mathbf{x}) < v(\mathbf{x}) < \operatorname{ess\,sup} h(\mathbf{x}), \quad \forall \mathbf{x} \in \Omega.$$

To utilize the boundedness of the operator $(\mathcal{I} - \nu\Delta)^{-1}$, we add and subtract an additional term $\frac{\epsilon^2}{\nu}\Delta u$ to Eq. (1.7), then a reformulation of the viscous Cahn–Hilliard equation is obtained [61]:

$$\begin{aligned}
\frac{\partial u}{\partial t} &= (\mathcal{I} - \nu\Delta)^{-1}\left[\left(\frac{\epsilon^2}{\nu}\mathcal{I} - \epsilon^2\Delta\right)\Delta u + \Delta\left(f(u) - \frac{\epsilon^2}{\nu}u\right)\right] \\
&= (\mathcal{I} - \nu\Delta)^{-1}\left[\frac{\epsilon^2}{\nu}(\mathcal{I} - \nu\Delta)\Delta u + \frac{1}{\nu}(\mathcal{I} + \nu\Delta - \mathcal{I})\left(f(u) - \frac{\epsilon^2}{\nu}u\right)\right] \\
&= \frac{\epsilon^2}{\nu}\Delta u + \frac{1}{\nu}\left[(\mathcal{I} - \nu\Delta)^{-1} - \mathcal{I}\right]\left(f(u) - \frac{\epsilon^2}{\nu}u\right) \\
&=: \mathcal{L}u + \mathcal{N}(u).
\end{aligned} \tag{2.1}$$

Considering the addition and subtraction of a stabilization term $-\kappa u$ $(\kappa \geq 0)$ to and from the viscous Cahn–Hilliard system (2.1), we obtain an equivalent form:

$$u_t = \mathcal{L}_\kappa u + \mathcal{N}_\kappa(u), \tag{2.2}$$

where $\mathcal{L}_\kappa = \mathcal{L} - \kappa\mathcal{I}$ and $\mathcal{N}_\kappa(u) = \mathcal{N}(u) + \kappa u$.

Letting $f_1(\xi) = f(\xi) - \frac{\epsilon^2}{\nu}\xi$, $f_2(\xi, \kappa) = (\frac{\epsilon^2}{\nu} + \nu\kappa)\xi - f(\xi)$, we assume $f_1$, $f_2$, and $f$ satisfy the following assumption.

**Assumption 2.1.** [61]

(1) There exists $m \leq m_- \leq \xi_- \leq \xi_+ \leq M_+ \leq M$ such that $f_1(m_-) = f_1(\xi_+) \leq f_1(\xi)$, $\forall \xi \geq m_-$; $f_1(M_+) = f_1(\xi_-) \geq f_1(\xi)$, $\forall \xi \leq M_+$, $f_1$ is strictly increasing for $\xi \in (m, m_-)$ and $\xi \in (M_+, M)$.
(2) There exists $\kappa^* \geq 0$, such that for any $\kappa \geq \kappa^*$, $f_2(\xi, \kappa)$ is strictly increasing for $\xi \in [m, M]$.
(3) The function $\nu^{-1} f_1(\xi)$ is Lipschitz continuous in $[m, M]$, i.e.,

$$\exists K > 0, \quad \text{such that } |\nu^{-1} f_1(\xi_1) - \nu^{-1} f_1(\xi_2)| \leq K|\xi_1 - \xi_2|.$$

Below we show that the potentials (1.2) and (1.3) satisfy Assumption 2.1.

**Lemma 2.2.** *For the Ginzburg–Landau polynomial potential (1.2), let $f_1(\xi) = \xi^3 - \xi - \frac{\epsilon^2}{\nu}\xi$ and $f_2(\xi, \kappa) = (\frac{\epsilon^2}{\nu} + \nu\kappa)\xi - \xi^3 + \xi$. If $\beta \geq \sqrt{\frac{4}{3}(1 + \frac{\epsilon^2}{\nu})}$, then*

$$\max_{|\xi| \leq \beta} |f_1(\xi)| \leq f_1(\beta). \tag{2.3}$$

*Furthermore, letting $\beta \geq \sqrt{\frac{1}{3}(1 + \frac{\epsilon^2}{\nu})}$ and $\kappa \geq \kappa^* = \frac{3\beta^2 - 1 - \epsilon^2/\nu}{\nu}$, $f_2(\xi, \kappa)$ is strictly increasing for $\xi \in [-\beta, \beta]$ and*

$$\max_{|\xi|\le\beta} |f_2(\xi,\kappa)| \le f_2(\beta,\kappa). \tag{2.4}$$

**Proof.** Calculating $f_1'(\xi)=0$, one can easily obtain two roots: $\xi_\pm = \pm\sqrt{\frac{1+\epsilon^2/\nu}{3}}$. Computing the positive root of $f_1(\xi) = f_1(\xi_-)$ yields $M_+ = \sqrt{\frac{4}{3}(1+\frac{\epsilon^2}{\nu})}$. Note that $f_1'(\xi)\ge 0,\ \forall \xi \ge \xi_+$, then $f_1(\beta) \ge f_1(M_+) = |f_1(\xi_\pm)|,\ \forall \beta \ge M_+$. The inequality (2.3) holds since $f_1(\xi)$ is an odd function.

Let us consider $\beta \ge \sqrt{\frac{1}{3}(1+\frac{\epsilon^2}{\nu})}$ and $\kappa \ge \kappa^* = \frac{3\beta^2-1-\epsilon^2/\nu}{\nu}$. When $|\xi|\le\beta$, it holds that $\frac{\partial}{\partial\xi} f_2(\xi,\kappa) = \frac{\epsilon^2}{\nu} + \nu\kappa - 3\xi^2 + 1 \ge 0$. Thus, $f_2(\xi,\kappa)$ is strictly increasing. Thanks to $f_2(\xi,\kappa)$ is an odd function about $\xi$, the inequality (2.4) holds. □

**Lemma 2.3.** *For the Flory–Huggins logarithmic potential, let* $f_1(\xi) = \frac{\theta}{2}\ln\frac{1+\xi}{1-\xi} - \theta_c\xi - \frac{\epsilon^2}{\nu}\xi$ *and* $\alpha_1 = \theta_c + \frac{\epsilon^2}{\nu}$. *If* $\beta \in [M_+, 1)$, *where* $M_+$ *is the positive root of* $f_1(\xi) = f_1(-\sqrt{1-\frac{\theta}{\alpha_1}})$, *then*

$$\max_{|\xi|\le\beta} |f_1(\xi)| \le f_1(\beta). \tag{2.5}$$

*Similarly, let* $f_2(\xi,\kappa) := -\frac{\theta}{2}\ln\frac{1+\xi}{1-\xi} + \theta_c\xi + (\frac{\epsilon^2}{\nu}+\nu\kappa)\xi$ *and* $\alpha_2 = \theta_c + \frac{\epsilon^2}{\nu} + \nu\kappa$. *If* $\beta \in [\sqrt{1-\frac{\theta}{\alpha_1}}, 1)$ *and* $\kappa \ge \kappa^* = \frac{1}{\nu}\big(\frac{\theta}{1-\beta^2} - \theta_c - \frac{\epsilon^2}{\nu}\big)$, *then* $f_2(\xi,\kappa)$ *is strictly increasing for* $\xi \in [-\beta,\beta]$ *and*

$$\max_{|\xi|\le\beta} |f_2(\xi,\kappa)| \le f_2(\beta,\kappa). \tag{2.6}$$

**Proof.** Calculating $f_1'(\xi)=0$ yields $\xi_\pm = \pm\sqrt{1-\frac{\theta}{\alpha_1}}$. Assume that $M_+$ is the positive root of the function $f_1(\xi) = f(-\sqrt{1-\frac{\theta}{\alpha_1}})$, and since $f_1'(\xi)\ge 0$, $\forall \xi \in [\xi_+, 1)$, it can be verified that $f_1(\beta) \ge f_1(M_+) = |f_1(\xi_\pm)|$ for any $\beta \in [M_+, 1)$. Note that $f_1(\xi)$ is an odd function, the inequality (2.5) holds.

Similarly, when $\beta \in [\sqrt{1-\frac{\theta}{\alpha_1}}, 1)$ and $\kappa \ge \kappa^* = \frac{1}{\nu}\left(\frac{\theta}{1-\beta^2} - \theta_c - \frac{\epsilon^2}{\nu}\right)$, we have $\frac{\partial}{\partial\xi} f_2(\xi,\kappa) = \alpha_2 - \frac{\theta}{1-\xi^2} \ge 0$. Thus, $f_2(\xi,\kappa)$ is strictly increasing for $\xi \in [-\beta,\beta]$. It is easy to verify that $f_2(-\xi,\kappa) = -f_2(\xi,\kappa)$, then the inequality (2.6) holds. □

Based on Lemmas 2.2 and 2.3, we obtain another important lemma as follows.

**Lemma 2.4.** *For the viscous Cahn–Hilliard equation (2.1) with periodic or homogeneous Neumann boundary conditions, the circle condition for* $\mathcal{N}(u)$ *holds; that is,*

$$\exists \kappa^* \ge 0, \text{ such that } \|\mathcal{N}_\kappa(u)\|_{L^\infty} \le \kappa\beta \text{ for any } \|u\|_{L^\infty} \le \beta \text{ and } \kappa \ge \kappa^*, \tag{2.7}$$

*where* $\beta$ *needs to satisfy the following condition given by Lemma 2.2 or Lemma 2.3:*

1. *for the Ginzburg–Landau polynomial potential:* $\beta \ge \sqrt{\frac{4}{3}(1+\frac{\epsilon^2}{\nu})}$;
2. *for the Flory–Huggins logarithmic potential:* $\beta \in [M^+, 1)$, *where* $M^+$ *is the positive root of* $f_1\left(-\sqrt{1-\frac{\theta}{\theta_c+\frac{\epsilon^2}{\nu}}}\right)$ *in Lemma 2.3.*

**Proof.** Here we give the proof for the Ginzburg–Landau polynomial potential, because the proof for the Flory–Huggins logarithmic potential is quite similar to it and so is omitted. Note that

$$\begin{aligned}
\mathcal{N}_\kappa(u) &= \mathcal{N}(u) + \kappa u = \kappa\left[u + \kappa^{-1}\mathcal{N}(u)\right] \\
&= \kappa\{u + (\kappa\nu)^{-1}\left[(\mathcal{I}-\nu\Delta)^{-1} - \mathcal{I}\right][f(u) - \frac{\epsilon^2}{\nu}u]\} \\
&= \nu^{-1}\{(\mathcal{I}-\nu\Delta)^{-1}[\underbrace{f(u) - \frac{\epsilon^2}{\nu}u}_{f_1(u)}] + [\underbrace{(\frac{\epsilon^2}{\nu}+\nu\kappa)u - f(u)}_{f_2(u,\kappa)}]\}.
\end{aligned}$$

Applying Lemma 2.2, when $\kappa \ge \kappa^*$ and $\beta \ge \sqrt{\frac{4}{3}(1+\frac{\epsilon^2}{\nu})}$, we always have $f_1(-\beta) \le f_1(u(\mathbf{x})) \le f_1(\beta)$ and $f_2(-\beta,\kappa) \le f_2(u(\mathbf{x}),\kappa) \le f_2(\beta,\kappa)$ for any $\|u\|_{L^\infty} \le \beta$. Then applying Lemma 2.1 yields

$$-\kappa\beta = \nu^{-1}\left[f_1(-\beta) + f_2(-\beta,\kappa)\right] \le \mathcal{N}_\kappa(u(\mathbf{x})) \le \nu^{-1}\left[f_1(\beta) + f_2(\beta,\kappa)\right] = \kappa\beta,$$

for almost all $\mathbf{x} \in \Omega$, (2.7) thus holds. □

**Remark 2.1.** When considering the Ginzburg–Landau polynomial potential (1.2) or Flory–Huggins logarithmic potential (1.3), the Lipschitz constant of $\nu^{-1} f_1(\xi)$ is calculated as $K = \nu^{-1} \max_{|\xi|\le\beta} |f_1'(\xi)|$. In fact, it is easy to see from Lemmas 2.2 and 2.3 that $\kappa^* = K$, i.e., the stabilization parameter $\kappa \ge K$, which will be used in the later proof.

Now we introduce the maximum principle of the viscous Cahn–Hilliard equation with either the Ginzburg–Landau polynomial potential (1.2) or Flory–Huggins logarithmic potential (1.3).

**Theorem 2.1.** *[61] Under periodic or homogeneous Neumann boundary conditions, the viscous Cahn–Hilliard equation has a unique solution $u \in C(0, T; L^\infty)$ and admits the maximum principle:*

1. *for the Ginzburg–Landau polynomial potential:* $\exists \beta = \max\left\{\sqrt{\frac{4}{3}\left(1+\frac{\epsilon^2}{\nu}\right)}, \|u^0\|_{L^\infty}\right\}$, *such that* $\|u(t)\|_{L^\infty} \le \beta, \forall t \in [0, T]$;
2. *for the Flory–Huggins logarithmic potential:* $\exists \beta = \max\left\{M^+, \|u^0\|_{L^\infty}\right\} < 1$, *such that* $\|u(t)\|_{L^\infty} \le \beta, \forall t \in [0, T]$,

*where $M^+$ is the positive root of $f_1\left(-\sqrt{1-\frac{\theta}{\theta_c+\frac{\epsilon^2}{\nu}}}\right)$ in Lemma 2.3.*

## 3. Stabilized exponential time differencing Runge–Kutta integrators

### 3.1. Spatial and temporal discretization

One popular spatial discretization that has been frequently adopted to preserve the maximum principle in the studies of phase-field models is the second-order finite difference method (see, e.g. [13,63,64,38,39,43]). We here consider the hypercube domain. For the one-dimensional (1D) interval $(a, b)$, setting the mesh size $h = \frac{b-a}{N}$ for periodic boundary conditions ($h = \frac{b-a}{N-1}$ for Neumann boundary conditions), we denote grid points as $\Omega_h = \{x_j | x_j = a + jh,\ \ j = 0, \cdots, N-1\}$ and the space of grid functions $\mathbb{V}_N = \{\boldsymbol{v} | \boldsymbol{v} = [v(x_0), \cdots, v(x_{N-1})]^T, x_j \in \Omega_h\} \subset \mathbb{R}^N$. Then, we obtain the ordinary differential equations (ODEs) system:

$$\frac{\mathrm{d}\boldsymbol{u}}{\mathrm{d}t} = L\boldsymbol{u} + N(\boldsymbol{u}), \quad \forall t \in (0, T], \tag{3.1}$$

where $\boldsymbol{u}$ is the grid function, $L\boldsymbol{u} = \frac{\epsilon^2}{\nu}\Delta_h \boldsymbol{u}$ and $N(\boldsymbol{u}) = \frac{1}{\nu}\left[(I - \nu\Delta_h)^{-1} - I\right]\left(f(\boldsymbol{u}) - \frac{\epsilon^2}{\nu}\boldsymbol{u}\right)$. Here, $I$ represents the identity matrix and $\Delta_h$ represents the central finite differentiation of $\Delta$, which has the form

$$\Delta_h = \frac{1}{h^2}\begin{bmatrix} -2 & 1 & & & 1 \\ 1 & -2 & 1 & & \\ & \ddots & \ddots & \ddots & \\ & & 1 & -2 & 1 \\ 1 & & & 1 & -2 \end{bmatrix}, \quad \Delta_h = \frac{1}{h^2}\begin{bmatrix} -2 & 2 & & & \\ 1 & -2 & 1 & & \\ & \ddots & \ddots & \ddots & \\ & & 1 & -2 & 1 \\ & & & 2 & -2 \end{bmatrix},$$

corresponding to periodic and homogeneous Neumann boundary conditions. By using the Kronecker tensor product, the two-dimensional (2D) and three-dimensional (3D) discrete matrices for the Laplace operator are straightforward. To save space, we omit them.

Now we present a family of first- and second-order ETDRK schemes. To briefly define the ETD methods, we introduce the functions

$$\varphi_k(z) = \int_0^1 e^{(1-s)z}\frac{s^{k-1}}{(k-1)!}\,ds > 0, \quad k \ge 1, \tag{3.2}$$

which satisfy the recursion relation

$$\varphi_k(z) = \frac{\varphi_{k-1}(z) - \frac{1}{(k-1)!}}{z}, \quad \varphi_0(z) = e^z. \tag{3.3}$$

We consider some Butcher-like tableaux corresponding to the first- (I) and second-order (II-IV) explicit ETDRK schemes [50,65]:

$$
\begin{aligned}
&\mathrm{I}: \begin{array}{c|c} 0 & 0 \\ \hline 1 & \varphi_1 \end{array}, \qquad
\mathrm{II}: \begin{array}{c|cc} 0 & 0 & \\ c_1 & c_1\varphi_{1,1} & 0 \\ \hline 1 & \varphi_1 - \frac{1}{c_1}\varphi_2 & \frac{1}{c_1}\varphi_2 \end{array}, \\
&\mathrm{III}: \begin{array}{c|cc} 0 & 0 & \\ c_1 & c_1\varphi_{1,1} & 0 \\ \hline 1 & (1-\frac{1}{2c_1})\varphi_1 & \frac{1}{2c_1}\varphi_1 \end{array}, \qquad
\mathrm{IV}: \begin{array}{c|ccc} 0 & 0 & & \\ c_1 & c_1\varphi_{1,1} & 0 & \\ 1 & \varphi_1 - \frac{1}{c_1}\varphi_2 & \frac{1}{c_1}\varphi_2 & 0 \\ \hline 1 & \varphi_1 - \varphi_2 & 0 & \varphi_2 \end{array},
\end{aligned} \tag{3.4}
$$

where the abscissas are required to satisfy $c_1 \geq 1$(II, IV), $c_1 \geq \frac{1}{2}$(III), and $\varphi_{k,i}(z) := \varphi_k(c_i z)$. For the sake of conciseness, we introduce a unified $s$-stage ($1 \leq s \leq 3$) formulation for the stabilized ETDRK schemes:

$$
\begin{cases}
\boldsymbol{u}_{n,0} = \boldsymbol{u}^n, \\
\boldsymbol{u}_{n,i} = \varphi_0(c_i\tau L_\kappa)\boldsymbol{u}^n + \tau \sum_{j=0}^{i-1} a_{i,j}(\tau L_\kappa) N_\kappa(\boldsymbol{u}_{n,j}), \quad i = 1, \cdots, s, \\
\boldsymbol{u}^{n+1} = \boldsymbol{u}_{n,s},
\end{cases} \tag{3.5}
$$

where the coefficient $a_{i,j}(z)$ is given in (3.4) for each scheme, $L_\kappa = L - \kappa I$, and $N_\kappa(\boldsymbol{u}) = N(\boldsymbol{u}) + \kappa \boldsymbol{u}$.

### 3.2. Preservation of the discrete maximum principle

First, let us introduce several essential lemmas which will be employed later.

**Lemma 3.1.** *[34] Let $B \in \mathbb{R}^{N\times N}$ and $A = aI - B$, where $a > 0$. If $B = (b_{ij})$ satisfies $b_{ii} = -b < 0$ and $b \geq \max_i \sum_{j\neq i} |b_{ij}|$, $0 \leq i \leq N-1$, then*

$$\|A^{-1}\|_\infty \leq \frac{1}{a},$$

*where the notation $\|\cdot\|_\infty$ represents the matrix $\infty$-norm.*

Immediately, we obtain $\|(I - \nu\Delta_h)^{-1}\|_\infty \leq 1$ and the following lemma.

**Lemma 3.2.** *For any $\|\boldsymbol{u}_j\|_{l^\infty} \leq \beta$ $(j = 1, 2)$, it holds that*

$$\|N_\kappa(\boldsymbol{u}_1) - N_\kappa(\boldsymbol{u}_2)\|_{l^\infty} \leq 3\kappa\|\boldsymbol{u}_1 - \boldsymbol{u}_2\|_{l^\infty}.$$

**Proof.** According to Assumption 2.1, Remark 2.1, and Lemma 3.1, it yields

$$
\begin{aligned}
\|N_\kappa(\boldsymbol{u}_1) - N_\kappa(\boldsymbol{u}_2)\|_{l^\infty} &= \|\kappa(\boldsymbol{u}_1 - \boldsymbol{u}_2) + \frac{1}{\nu}(I - \nu\Delta_h)^{-1}[f_1(\boldsymbol{u}_1) - f_1(\boldsymbol{u}_2)] - \frac{1}{\nu}f_1(\boldsymbol{u}_1) + \frac{1}{\nu}f_1(\boldsymbol{u}_2)\|_{l^\infty} \\
&\leq \kappa\|\boldsymbol{u}_1 - \boldsymbol{u}_2\|_{l^\infty} + \frac{1}{\nu}\|(I - \nu\Delta_h)^{-1}\|_\infty \|f_1(\boldsymbol{u}_1) - f_1(\boldsymbol{u}_2)\|_{l^\infty} \\
&\quad + \frac{1}{\nu}\|f_1(\boldsymbol{u}_1) - f_1(\boldsymbol{u}_2)\|_{l^\infty} \\
&\leq \kappa\|\boldsymbol{u}_1 - \boldsymbol{u}_2\|_{l^\infty} + 2K\|\boldsymbol{u}_1 - \boldsymbol{u}_2\|_{l^\infty} \\
&\leq \kappa\|\boldsymbol{u}_1 - \boldsymbol{u}_2\|_{l^\infty} + 2\kappa\|\boldsymbol{u}_1 - \boldsymbol{u}_2\|_{l^\infty} \\
&= 3\kappa\|\boldsymbol{u}_1 - \boldsymbol{u}_2\|_{l^\infty}. \quad \square
\end{aligned}
$$

**Lemma 3.3.** *For any $z \neq 0$, it holds that $\varphi_0(z) - z\varphi_1(z) = 1$.*

**Proof.** This equality is obvious by setting $k = 1$ in Eq. (3.3). $\square$

**Lemma 3.4.** *[39] For any $c_i\tau\kappa > 0$, it holds that*

$$\|\varphi_0(c_i\tau L_\kappa)\|_\infty = \varphi_0(-c_i\tau\kappa) < 1,$$

*and every entry of $\varphi_0(c_i\tau L_\kappa)$ is non-negative.*

**Lemma 3.5.** *[66] For any $\kappa > 0$ and $\tau > 0$, it holds that*

$$\|\varphi_j(\tau L_\kappa)\|_\infty = \varphi_j(-\tau\kappa) = \frac{1}{\tau^j}\int_0^\tau e^{-(\tau-s)\kappa}\frac{s^{j-1}}{(j-1)!}ds < \frac{1}{j!}, \quad \forall j \geq 1,$$

$$\|\varphi_1(\tau L_\kappa) - \frac{1}{c_1}\varphi_2(\tau L_\kappa)\|_\infty = \varphi_1(-\tau\kappa) - \frac{1}{c_1}\varphi_2(-\tau\kappa), \quad \forall c_1 \geq 1.$$

**Lemma 3.6.** *[66] For the matrix $L_\kappa$, it holds that:*

$$\langle\varphi_j(\tau L_\kappa)\boldsymbol{u}, \mathbf{1}\rangle_h = \varphi_j(-\tau\kappa)\langle\boldsymbol{u}, \mathbf{1}\rangle_h, \quad \forall\tau > 0,\ j \geq 1,$$

*where $\mathbf{1} = [1, \cdots, 1]^T \in \mathbb{R}^N$ for periodic boundary conditions, and $\mathbf{1} = [\frac{1}{2}, 1, \cdots, 1, \frac{1}{2}]^T$ for homogeneous Neumann boundary conditions in 1D, and the notation $\langle\cdot,\cdot\rangle_h$ denotes the $l^2$ inner product, which is defined as*

$$\langle\boldsymbol{u}, \boldsymbol{v}\rangle_h := h^d\boldsymbol{v}^T\boldsymbol{u} = h^d\sum_{j=0}^{N-1}u_j v_j, \quad \forall\boldsymbol{u}, \boldsymbol{v} \in \mathbb{V}_N.$$

Now we show that the stabilized ETDRK schemes unconditionally preserve the discrete maximum principle.

**Theorem 3.1.** *Suppose that the initial value of system (2.2) satisfies $\|\boldsymbol{u}^0\|_{l^\infty} \leq \beta$. Under Assumption 2.1, the stabilized ETDRK schemes with $\kappa \geq \kappa^* = K$ given by (3.5) preserve the discrete maximum principle unconditionally in the sense that $\|\boldsymbol{u}^n\|_{l^\infty} \leq \beta$ for any $\tau > 0$.*

**Proof.** We prove this theorem by a mathematical induction argument. Assuming $\|\boldsymbol{u}_{n,j}\|_{l^\infty} \leq \beta,\ j = 0, \cdots, i-1$, we verify that the result holds for $\boldsymbol{u}_{n,i},\ i \leq s$.

In particular, for each Butcher tableau in (3.4), summing $a_{i,j}(-\tau\kappa)$ over $j$ yields

$$\sum_{j=0}^{i-1}a_{i,j}(-\tau\kappa) = c_i\varphi_1(-c_i\tau\kappa), \quad i = 1, \cdots, s. \tag{3.6}$$

For each stage of (3.5), by using Lemmas 2.4, 3.2–3.4, and Eq. (3.6), we have

$$\begin{aligned}
\|\boldsymbol{u}_{n,i}\|_{l^\infty} &= \|\varphi_0(c_i\tau L_\kappa)\boldsymbol{u}^n + \tau\sum_{j=0}^{i-1}a_{i,j}(\tau L_\kappa)N_\kappa(\boldsymbol{u}_{n,j})\|_{l^\infty} \\
&\leq \|\varphi_0(c_i\tau L_\kappa)\|_\infty\|u^n\|_{l^\infty} + \tau\sum_{j=0}^{i-1}\|a_{i,j}(\tau L_\kappa)\|_\infty\|N_\kappa(\boldsymbol{u}_{n,j})\|_{l^\infty} \\
&\leq [\varphi_0(-c_i\tau\kappa) + \tau\kappa\sum_{j=0}^{i-1}a_{i,j}(-\tau\kappa)]\beta \\
&= [\varphi_0(-c_i\tau\kappa) + c_i\tau\kappa\varphi_1(-c_i\tau\kappa)]\,\beta \\
&= \beta, \quad i \leq s.
\end{aligned}$$

Thus, we obtain $\|\boldsymbol{u}^{n+1}\|_{l^\infty} = \|\boldsymbol{u}_{n,s}\|_{l^\infty} \leq \beta$. This completes the proof. □

**Remark 3.1.** The key of this proof is the positivity of the coefficients $a_{i,j}(\cdot)$ in the corresponding Butcher-like tableau, and such methods are denoted as positive ETDRK methods. However, it has been proven that the positive ETDRK and ETDMS schemes have a second-order barrier [67,68]. Consequently, the unconditionally MPP schemes are limited to the second order.

### 3.3. Preservation of the mass conservation law

Next, we show that the stabilized ETDRK schemes unconditionally preserve the mass conservation law for the viscous Cahn–Hilliard equation.

**Theorem 3.2.** *Under periodic or homogeneous Neumann boundary conditions and Assumption 2.1, the stabilized ETDRK schemes given by (3.5) preserve the mass conservation law unconditionally for the viscous Cahn–Hilliard equation (2.1), namely, for any $\tau > 0$, the stabilized ETDRK (I-IV) schemes satisfy*

$$\langle \boldsymbol{u}^{n+1}, \mathbf{1}\rangle_h = \langle \boldsymbol{u}^{n}, \mathbf{1}\rangle_h = \cdots = \langle \boldsymbol{u}^{0}, \mathbf{1}\rangle_h.$$

**Proof.** We prove this by induction. Assuming $\langle \boldsymbol{u}_{n,j}, \mathbf{1}\rangle_h = \langle \boldsymbol{u}^0, \mathbf{1}\rangle_h$, $j = 0, \cdots, i-1$, we verify that the result holds for $\boldsymbol{u}^{n+1}$. Denoting $(I - \nu\Delta_h)^{-1} f_1(\boldsymbol{u})$ by $g(\boldsymbol{u})$, we have

$$\langle f_1(\boldsymbol{u}), \mathbf{1}\rangle_h = \langle (I - \nu\Delta_h) g(\boldsymbol{u}), \mathbf{1}\rangle_h = \langle g(\boldsymbol{u}), \mathbf{1}\rangle_h - \nu\langle \Delta_h g(\boldsymbol{u}), \mathbf{1}\rangle_h = \langle g(\boldsymbol{u}), \mathbf{1}\rangle_h,$$

under periodic or homogeneous Neumann boundary conditions, then the following property holds for the nonlinear term of the viscous Cahn–Hilliard equation (2.1):

$$\langle N(\boldsymbol{u}), \mathbf{1}\rangle_h = \frac{1}{\nu}\left[\langle g(\boldsymbol{u}), \mathbf{1}\rangle_h - \langle f_1(\boldsymbol{u}), \mathbf{1}\rangle_h\right] = 0.$$

By taking the $l^2$ inner product on both sides of (3.5) with the vector $\mathbf{1}$, applying the above property, and Lemmas 3.3 and 3.6, we obtain

$$\begin{aligned}
\langle \boldsymbol{u}_{n,i}, \mathbf{1}\rangle_h &= \langle \varphi_0(c_i\tau L_\kappa)\boldsymbol{u}^n + \tau\sum_{j=0}^{i-1} a_{i,j}(\tau L_\kappa) N_\kappa(\boldsymbol{u}_{n,j}), \mathbf{1}\rangle_h \\
&= \langle \varphi_0(-c_i\tau\kappa)\boldsymbol{u}^n + \tau\sum_{j=0}^{i-1} a_{i,j}(-\tau\kappa)\kappa\boldsymbol{u}_{n,j}, \mathbf{1}\rangle_h \\
&= \langle [\varphi_0(-c_i\tau\kappa) + c_i\tau\kappa\varphi_1(-c_i\tau\kappa)]\boldsymbol{u}^n, \mathbf{1}\rangle_h \\
&= \left\langle \boldsymbol{u}^n, \mathbf{1}\right\rangle_h, \quad i \le s.
\end{aligned}$$

Thus, we obtain $\langle \boldsymbol{u}^{n+1}, \mathbf{1}\rangle_h = \langle \boldsymbol{u}_{n,s}, \mathbf{1}\rangle_h = \langle \boldsymbol{u}^0, \mathbf{1}\rangle_h$, and the proof is completed. □

### 3.4. Preservation of the energy dissipation law

It is often viewed that the preservation of energy dissipation not only preserves the physical feature but also provides stability to the numerical simulation. Ju et al. [69] and Du et al. [57] proved that ETD I unconditionally preserves the energy dissipation law for the epitaxial growth model without slope selection and the nonlocal Allen–Cahn equation, respectively. Fu and Yang [70] proved that ETD II ($c_1 = 1$) can maintain energy dissipation unconditionally for a family of phase-field models, such as the Allen–Cahn equation, the Cahn–Hilliard equation, and the MBE model. In what follows we prove that a specific family of stabilized ETDRK schemes given by (3.5) unconditionally preserve the energy dissipation law for the viscous Cahn–Hilliard equation.

We denote by $H$ the discrete counterpart of the nonstandard Hilbert space $\mathcal{H}$; that is, $H := \{\boldsymbol{u} \in l^2(\mathbb{V}_N) | \langle \boldsymbol{u}, \mathbf{1}\rangle_h = 0\}$. Then, $-\Delta_h$ is self-adjoint and positive definite on $H$. Therefore, the discrete analogue of the operator $\mathcal{A}$ in Section 1 is represented as $A_h^{-1} := -(I - \nu\Delta_h)\Delta_h^{-1} = -(\Delta_h)^{-1} + \nu I$, which is positive definite on $H$. Moreover, for any $\boldsymbol{u}, \boldsymbol{v} \in H$, we define the discrete $H$ inner product as

$$\langle \boldsymbol{u}, \boldsymbol{v}\rangle_H = \langle \boldsymbol{u}, (-\Delta_h)^{-1}\boldsymbol{v}\rangle_h + \nu\langle \boldsymbol{u}, \boldsymbol{v}\rangle_h = \langle A_h^{-1}\boldsymbol{u}, \boldsymbol{v}\rangle_h.$$

**Theorem 3.3.** *When $c_1 = 1$ and $\kappa \ge K$, the stabilized ETDRK schemes given by (3.5) unconditionally decrease the energy of the viscous Cahn–Hilliard equation (2.1); that is,*

$$E(\boldsymbol{u}^{n+1}) \le E(\boldsymbol{u}^n), \quad \forall \tau > 0.$$

**Proof.** (1) Proof for ETD I.

By adding and subtracting an auxiliary term $\frac{\epsilon^2}{2\nu}\boldsymbol{u}^2$ to the energy, we obtain a natural splitting of the energy $E(\boldsymbol{u}) = E_l(\boldsymbol{u}) + E_n(\boldsymbol{u})$, with

$$\begin{aligned}
E_l(\boldsymbol{u}) &= -\frac{\epsilon^2}{2}\langle \boldsymbol{u}, \Delta_h\boldsymbol{u}\rangle_h + \frac{\epsilon^2}{2\nu}\langle \boldsymbol{u}, \boldsymbol{u}\rangle_h, \\
E_n(\boldsymbol{u}) &= \langle F(\boldsymbol{u}) - \frac{\epsilon^2}{2\nu}\boldsymbol{u}^2, \mathbf{1}\rangle_h.
\end{aligned}$$

Differencing the two energy functionals $E_l(\boldsymbol{v})$ and $E_l(\boldsymbol{u})$ yields

$$
\begin{aligned}
E_l(\boldsymbol{v}) - E_l(\boldsymbol{u}) &= -\frac{\epsilon^2}{2}\left(\langle \boldsymbol{v}, \Delta_h \boldsymbol{v}\rangle_h - \langle \boldsymbol{u}, \Delta_h \boldsymbol{u}\rangle_h\right) + \frac{\epsilon^2}{2\nu}\left(\langle \boldsymbol{v}, \boldsymbol{v}\rangle_h - \langle \boldsymbol{u}, \boldsymbol{u}\rangle_h\right) \\
&= -\epsilon^2\langle \boldsymbol{v}-\boldsymbol{u}, \Delta_h \boldsymbol{v}\rangle_h + \frac{\epsilon^2}{2}\langle \boldsymbol{v}-\boldsymbol{u}, \Delta_h(\boldsymbol{v}-\boldsymbol{u})\rangle_h + \frac{\epsilon^2}{\nu}\langle \boldsymbol{v}-\boldsymbol{u}, \boldsymbol{v}\rangle_h - \frac{\epsilon^2}{2\nu}\langle \boldsymbol{v}-\boldsymbol{u}, \boldsymbol{v}-\boldsymbol{u}\rangle_h \\
&\le -\epsilon^2\langle \boldsymbol{v}-\boldsymbol{u}, \Delta_h \boldsymbol{v}\rangle_h + \frac{\epsilon^2}{\nu}\langle \boldsymbol{v}-\boldsymbol{u}, \boldsymbol{v}\rangle_h \\
&= -\nu\langle \boldsymbol{v}-\boldsymbol{u}, L_\kappa \boldsymbol{v}\rangle_h - \nu\kappa\langle \boldsymbol{v}-\boldsymbol{u}, \boldsymbol{v}\rangle_h + \frac{\epsilon^2}{\nu}\langle \boldsymbol{v}-\boldsymbol{u}, \boldsymbol{v}\rangle_h,
\end{aligned} \tag{3.7}
$$

where $L_\kappa \boldsymbol{v} = \frac{\epsilon^2}{\nu}\Delta_h \boldsymbol{v} - \kappa \boldsymbol{v}$ and the identity

$$\langle a, a\rangle - \langle b, b\rangle = 2\langle a-b, a\rangle - \langle a-b, a-b\rangle$$

is used.

For $E_n(\boldsymbol{v})$ and $E_n(\boldsymbol{u})$, by using Taylor's expansion, we obtain

$$
\begin{aligned}
E_n(\boldsymbol{v}) - E_n(\boldsymbol{u}) &= \langle \boldsymbol{v}-\boldsymbol{u}, f_1(\boldsymbol{u})\rangle_h + \frac{1}{2}\langle \boldsymbol{v}-\boldsymbol{u}, f_1{}'(\boldsymbol{\xi})(\boldsymbol{v}-\boldsymbol{u})\rangle_h \\
&\le -\left\langle \boldsymbol{v}-\boldsymbol{u}, A_h^{-1}\left[N_\kappa(\boldsymbol{u}) - \kappa \boldsymbol{u}\right]\right\rangle_h + \frac{\nu}{2}K\langle \boldsymbol{v}-\boldsymbol{u}, \boldsymbol{v}-\boldsymbol{u}\rangle_h \\
&\le -\left\langle \boldsymbol{v}-\boldsymbol{u}, A_h^{-1}\left[N_\kappa(\boldsymbol{u}) - \kappa \boldsymbol{u}\right]\right\rangle_h + \frac{\nu}{2}\kappa\langle \boldsymbol{v}-\boldsymbol{u}, \boldsymbol{v}-\boldsymbol{u}\rangle_h,
\end{aligned} \tag{3.8}
$$

where $N_\kappa(\boldsymbol{u}) = (I - \nu\Delta_h)^{-1}\Delta_h f_1(\boldsymbol{u}) + \kappa \boldsymbol{u} = -A_h f_1(\boldsymbol{u}) + \kappa \boldsymbol{u}$ and the last term $\frac{\nu}{2}\kappa\langle \boldsymbol{v}-\boldsymbol{u}, \boldsymbol{v}-\boldsymbol{u}\rangle_h$ is based on Assumption 2.1 ($\kappa \ge K$).

Combining Eqs. (3.7) and (3.8) leads to

$$
\begin{aligned}
E(\boldsymbol{v}) - E(\boldsymbol{u}) &\le -\nu\langle \boldsymbol{v}-\boldsymbol{u}, L_\kappa \boldsymbol{v}\rangle_h - \nu\kappa\langle \boldsymbol{v}-\boldsymbol{u}, \boldsymbol{v}\rangle_h + \frac{\epsilon^2}{\nu}\langle \boldsymbol{v}-\boldsymbol{u}, \boldsymbol{v}\rangle_h \\
&\quad - \left\langle \boldsymbol{v}-\boldsymbol{u}, A_h^{-1}\left[N_\kappa(\boldsymbol{u}) - \kappa \boldsymbol{u}\right]\right\rangle_h + \frac{\nu}{2}\kappa\langle \boldsymbol{v}-\boldsymbol{u}, \boldsymbol{v}-\boldsymbol{u}\rangle_h \\
&= -\nu\langle \boldsymbol{v}-\boldsymbol{u}, L_\kappa \boldsymbol{v}\rangle_h - \nu\kappa\langle \boldsymbol{v}-\boldsymbol{u}, \boldsymbol{v}\rangle_h + \frac{\epsilon^2}{\nu}\langle \boldsymbol{v}-\boldsymbol{u}, \boldsymbol{v}\rangle_h \\
&\quad + \left\langle \boldsymbol{v}-\boldsymbol{u}, (\Delta_h^{-1} - \nu I)\left[N_\kappa(\boldsymbol{u}) - \kappa \boldsymbol{u}\right]\right\rangle_h + \frac{\nu}{2}\kappa\langle \boldsymbol{v}-\boldsymbol{u}, \boldsymbol{v}-\boldsymbol{u}\rangle_h \\
&= -\nu\langle \boldsymbol{v}-\boldsymbol{u}, L_\kappa \boldsymbol{v} + N_\kappa(\boldsymbol{u})\rangle_h + \langle \boldsymbol{v}-\boldsymbol{u}, \Delta_h^{-1}N(\boldsymbol{u}) + \frac{\epsilon^2}{\nu}\boldsymbol{v}\rangle_h - \frac{\nu}{2}\kappa\langle \boldsymbol{v}-\boldsymbol{u}, \boldsymbol{v}-\boldsymbol{u}\rangle_h \\
&\le -\nu\langle \boldsymbol{v}-\boldsymbol{u}, L_\kappa \boldsymbol{v} + N_\kappa(\boldsymbol{u})\rangle_h + \left\langle \boldsymbol{v}-\boldsymbol{u}, \Delta_h^{-1}\left[L\boldsymbol{v} + N(\boldsymbol{u})\right]\right\rangle_h \\
&= -\nu\langle \boldsymbol{v}-\boldsymbol{u}, L_\kappa \boldsymbol{v} + N_\kappa(\boldsymbol{u})\rangle_h + \left\langle \boldsymbol{v}-\boldsymbol{u}, \Delta_h^{-1}\left[L_\kappa \boldsymbol{v} + N_\kappa(\boldsymbol{u})\right]\right\rangle_h + \underbrace{\kappa\langle \boldsymbol{v}-\boldsymbol{u}, \Delta_h^{-1}(\boldsymbol{v}-\boldsymbol{u})\rangle_h}_{\le 0} \\
&\le -\left\langle \boldsymbol{v}-\boldsymbol{u}, A_h^{-1}\left[L_\kappa \boldsymbol{v} + N_\kappa(\boldsymbol{u})\right]\right\rangle_h, \\
&= -\left\langle \boldsymbol{v}-\boldsymbol{u}, \left[L_\kappa \boldsymbol{v} + N_\kappa(\boldsymbol{u})\right]\right\rangle_H.
\end{aligned} \tag{3.9}
$$

Using the equality $\varphi_1(\tau L_\kappa) = (\tau L_\kappa)^{-1}\left[\varphi_0(\tau L_\kappa) - I\right]$, and denoting $\varphi_k(\tau L_\kappa)$ by $\varphi_k$ for short, we have

$$
\begin{aligned}
E(\boldsymbol{u}^{n+1}) - E(\boldsymbol{u}^n) &\le -\left\langle \boldsymbol{u}^{n+1} - \boldsymbol{u}^n, \left[L_\kappa \boldsymbol{u}^{n+1} + N_\kappa(\boldsymbol{u}^n)\right]\right\rangle_H \\
&= -\left\langle \boldsymbol{u}^{n+1} - \boldsymbol{u}^n, \left[L_\kappa \boldsymbol{u}^{n+1} + (\tau\varphi_1)^{-1}(\boldsymbol{u}^{n+1} - \boldsymbol{u}^n + (1-\varphi_0)\boldsymbol{u}^n)\right]\right\rangle_H \\
&= -\left\langle \boldsymbol{u}^{n+1} - \boldsymbol{u}^n, \left[L_\kappa \boldsymbol{u}^{n+1} + (\tau\varphi_1)^{-1}(\boldsymbol{u}^{n+1} - \boldsymbol{u}^n) - L_\kappa \boldsymbol{u}^n\right]\right\rangle_H \\
&= -\left\langle \boldsymbol{u}^{n+1} - \boldsymbol{u}^n, \left[L_\kappa + (\tau\varphi_1)^{-1}\right](\boldsymbol{u}^{n+1} - \boldsymbol{u}^n)\right\rangle_H \\
&=: \left\langle \boldsymbol{u}^{n+1} - \boldsymbol{u}^n, \Delta_1(\boldsymbol{u}^{n+1} - \boldsymbol{u}^n)\right\rangle_h,
\end{aligned} \tag{3.10}
$$

where $\Delta_1 = -\tau^{-1}A_h^{-1}y_1(\tau L_\kappa)$ with $y_1(z) = z + [\varphi_1(z)]^{-1} = \frac{ze^z}{e^z-1}$. Note that both $L_\kappa$ and $-A_h^{-1}$ are negative definite and $y_1(z) > 0$ for any $z \ne 0$. Thus, $\Delta_1$ is negative definite, and $E(\boldsymbol{u}^{n+1}) - E(\boldsymbol{u}^n) \le 0$.

(2) Proof for ETD II.

Similarly, the first-stage solution $\boldsymbol{u}_{n,1}$ satisfies the inequality (3.10).

Continuing in this manner, we compute the energy difference between the final solution $\boldsymbol{u}^{n+1}$ and the stage solution $\boldsymbol{u}_{n,1}$:

$$\begin{aligned}
&E(\boldsymbol{u}^{n+1}) - E(\boldsymbol{u}_{n,1}) \le -\left\langle \boldsymbol{u}^{n+1} - \boldsymbol{u}_{n,1}, L_\kappa \boldsymbol{u}^{n+1} + N_\kappa(\boldsymbol{u}_{n,1})\right\rangle_H \\
&= -\left\langle \boldsymbol{u}^{n+1} - \boldsymbol{u}_{n,1}, L_\kappa \boldsymbol{u}^{n+1} - L_\kappa \boldsymbol{u}_{n,1} + (\tau\varphi_2)^{-1}(\boldsymbol{u}^{n+1} - \boldsymbol{u}_{n,1}) + L_\kappa \boldsymbol{u}_{n,1} + N_\kappa(\boldsymbol{u}^n)\right\rangle_H \\
&= -\left\langle \boldsymbol{u}^{n+1} - \boldsymbol{u}_{n,1}, \left[L_\kappa + (\tau\varphi_2)^{-1}\right](\boldsymbol{u}^{n+1} - \boldsymbol{u}_{n,1})\right\rangle_H + \left\langle \boldsymbol{u}^{n+1} - \boldsymbol{u}_{n,1}, \Delta_1(\boldsymbol{u}_{n,1} - \boldsymbol{u}^n)\right\rangle_h \\
&=: \left\langle \boldsymbol{u}^{n+1} - \boldsymbol{u}_{n,1}, \Delta_2(\boldsymbol{u}^{n+1} - \boldsymbol{u}_{n,1})\right\rangle_h + \left\langle \boldsymbol{u}^{n+1} - \boldsymbol{u}_{n,1}, \Delta_1(\boldsymbol{u}_{n,1} - \boldsymbol{u}^n)\right\rangle_h,
\end{aligned} \tag{3.11}$$

where $\Delta_2 = -\tau^{-1}A_h^{-1}y_2(\tau L_\kappa)$ with $y_2(z) = z + [\varphi_2(z)]^{-1} = \dfrac{z(e^z-1)}{e^z - z - 1}$. Since $y_2 > 0$ for any $z \neq 0$, $\Delta_2$ is negative definite.

Adding (3.10) to (3.11) leads to

$$\begin{aligned}
E(\boldsymbol{u}^{n+1}) - E(\boldsymbol{u}^n) \le &\underbrace{\left\langle \boldsymbol{u}^{n+1} - \boldsymbol{u}^n, \Delta_1(\boldsymbol{u}^{n+1} - \boldsymbol{u}^n)\right\rangle_h}_{A} + \underbrace{\left\langle \boldsymbol{u}^{n+1} - \boldsymbol{u}_{n,1}, \Delta_2(\boldsymbol{u}^{n+1} - \boldsymbol{u}_{n,1})\right\rangle_h}_{B} \\
&+ \underbrace{\left\langle \boldsymbol{u}^{n+1} - \boldsymbol{u}_{n,1}, \Delta_1(\boldsymbol{u}_{n,1} - \boldsymbol{u}^n)\right\rangle_h}_{C},
\end{aligned}$$

where

$$B = \underbrace{\left\langle \boldsymbol{u}^{n+1} - \boldsymbol{u}_{n,1}, \Delta_1\left(\boldsymbol{u}^{n+1} - \boldsymbol{u}_{n,1}\right)\right\rangle_h}_{B_1} + \underbrace{\langle \boldsymbol{u}^{n+1} - \boldsymbol{u}_{n,1}, (\Delta_2 - \Delta_1)\left(\boldsymbol{u}^{n+1} - \boldsymbol{u}_{n,1}\right)\rangle_h}_{B_2}.$$

Here, $\Delta_2 - \Delta_1 = -\tau^{-1}A_h^{-1}y_3(\tau L_\kappa)$, with

$$y_3(z) = y_2(z) - y_1(z) = \frac{1}{\varphi_2(z)} - \frac{1}{\varphi_1(z)} = \frac{z(ze^z - e^z + 1)}{(e^z - 1)(e^z - z - 1)}.$$

Simple calculations verify that $\dfrac{z}{e^z - 1} > 0$, $ze^z - e^z + 1 > 0$, and $e^z - z - 1 > 0$ for any $z \neq 0$. Thus, $y_3(z) > 0$, $\forall z \neq 0$, $\Delta_2 - \Delta_1$ is negative definite and $B \le 0$. Note that

$$\frac{1}{2}(A + C) = \frac{1}{2}\langle \boldsymbol{u}^{n+1} - \boldsymbol{u}^n, \Delta_1(\boldsymbol{u}_{n,1} - \boldsymbol{u}^n)\rangle_h, \quad \frac{1}{2}(B_1 + C) = \frac{1}{2}\langle \boldsymbol{u}^{n+1} - \boldsymbol{u}_{n,1}, \Delta_1(\boldsymbol{u}^{n+1} - \boldsymbol{u}^n)\rangle_h,$$

then,

$$\frac{1}{2}(A + B_1) + C = \frac{1}{2}\langle \boldsymbol{u}^{n+1} - \boldsymbol{u}^n, \Delta_1(\boldsymbol{u}^{n+1} - \boldsymbol{u}^n)\rangle_h \le 0.$$

Thus,

$$E(\boldsymbol{u}^{n+1}) - E(\boldsymbol{u}^n) \le \frac{1}{2}A + (\frac{1}{2}A + B_1) + C + \frac{1}{2}B_1 + B_2 \le 0.$$

(3) Proof for ETD III.

The first-stage solution $\boldsymbol{u}_{n,1}$ also satisfies the inequality (3.10).

For the final solution $\boldsymbol{u}^{n+1}$, it follows that:

$$\begin{aligned}
&E(\boldsymbol{u}^{n+1}) - E(\boldsymbol{u}_{n,1}) \le -\left\langle \boldsymbol{u}^{n+1} - \boldsymbol{u}_{n,1}, L_\kappa \boldsymbol{u}^{n+1} + N_\kappa(\boldsymbol{u}_{n,1})\right\rangle_H \\
&= -\left\langle \boldsymbol{u}^{n+1} - \boldsymbol{u}_{n,1}, L_\kappa \boldsymbol{u}^{n+1} - L_\kappa \boldsymbol{u}_{n,1} + L_\kappa \boldsymbol{u}_{n,1} + N_\kappa(\boldsymbol{u}^n) + (\frac{\tau}{2}\varphi_1)^{-1}\left(\boldsymbol{u}^{n+1} - \boldsymbol{u}_{n,1}\right)\right\rangle_H \\
&= -\left\langle \boldsymbol{u}^{n+1} - \boldsymbol{u}_{n,1}, \left[L_\kappa + (\frac{\tau}{2}\varphi_1)^{-1}\right]\left(\boldsymbol{u}^{n+1} - \boldsymbol{u}_{n,1}\right)\right\rangle_H + \left\langle \boldsymbol{u}^{n+1} - \boldsymbol{u}_{n,1}, \Delta_1(\boldsymbol{u}_{n,1} - \boldsymbol{u}^n)\right\rangle_h \\
&=: \left\langle \boldsymbol{u}^{n+1} - \boldsymbol{u}_{n,1}, \Delta_3\left(\boldsymbol{u}^{n+1} - \boldsymbol{u}_{n,1}\right)\right\rangle_h + \left\langle \boldsymbol{u}^{n+1} - \boldsymbol{u}_{n,1}, \Delta_1(\boldsymbol{u}_{n,1} - \boldsymbol{u}^n)\right\rangle_h,
\end{aligned} \tag{3.12}$$

where $\Delta_3 = -\tau^{-1}A_h^{-1}y_4(\tau L_\kappa)$, with $y_4(z) = z + 2[\varphi_1(z)]^{-1} = \frac{ze^z + z}{e^z - 1}$. Since $y_4(z) > 0$ for any $z \neq 0$, $\Delta_3$ is negative definite.

Adding (3.10) to (3.12) yields

$$\begin{aligned}
E(\boldsymbol{u}^{n+1}) - E(\boldsymbol{u}^n) \le &\underbrace{\left\langle \boldsymbol{u}_{n,1} - \boldsymbol{u}^n, \Delta_1(\boldsymbol{u}_{n,1} - \boldsymbol{u}^n)\right\rangle_h}_{A} + \underbrace{\left\langle \boldsymbol{u}^{n+1} - \boldsymbol{u}_{n,1}, \Delta_3\left(\boldsymbol{u}^{n+1} - \boldsymbol{u}_{n,1}\right)\right\rangle_h}_{B} \\
&+ \underbrace{\left\langle \boldsymbol{u}^{n+1} - \boldsymbol{u}_{n,1}, \Delta_1(\boldsymbol{u}_{n,1} - \boldsymbol{u}^n)\right\rangle_h}_{C},
\end{aligned}$$

where

$$B=\underbrace{\frac{1}{2}\left\langle \boldsymbol{u}^{n+1}-\boldsymbol{u}_{n,1},\Delta_1\left(\boldsymbol{u}^{n+1}-\boldsymbol{u}_{n,1}\right)\right\rangle_h}_{B_1}+\underbrace{\langle \boldsymbol{u}^{n+1}-\boldsymbol{u}_{n,1},(\Delta_3-\frac{1}{2}\Delta_1)\left(\boldsymbol{u}^{n+1}-\boldsymbol{u}_{n,1}\right)\rangle_h}_{B_2}.$$

Here, $\Delta_3-\frac{1}{2}\Delta_1=-\tau^{-1}A_h^{-1}y_5(\tau L_\kappa)$, with $y_5(z)=y_4(z)-\frac{1}{2}y_1(z)=\frac{z}{2}+\frac{3}{2}[\varphi_1(z)]^{-1}=\dfrac{ze^z+2z}{2(e^z-1)}$. It can be verified that $y_5(z)>0$ for any $z\neq 0$. Therefore, $\Delta_3-\frac{1}{2}\Delta_1$ is negative definite and $B_2\leq 0$.

Note that

$$\frac{1}{2}(A+C)=\frac{1}{2}\langle \boldsymbol{u}^{n+1}-\boldsymbol{u}^n,\Delta_1(\boldsymbol{u}_{n,1}-\boldsymbol{u}^n)\rangle_h,\quad B_1+\frac{1}{2}C=\frac{1}{2}\langle \boldsymbol{u}^{n+1}-\boldsymbol{u}_{n,1},\Delta_1(\boldsymbol{u}^{n+1}-\boldsymbol{u}^n)\rangle_h,$$

then,

$$\frac{1}{2}A+B_1+C=\frac{1}{2}\langle \boldsymbol{u}^{n+1}-\boldsymbol{u}^n,\Delta_1(\boldsymbol{u}^{n+1}-\boldsymbol{u}^n)\rangle_h\leq 0.$$

Thus,

$$E(\boldsymbol{u}^{n+1})-E(\boldsymbol{u}^n)\leq\frac{1}{2}A+(\frac{1}{2}A+B_1+C)+B_2\leq 0.$$

(4) Proof for ETD IV.

The first-stage solution $\boldsymbol{u}_{n,1}$ and the second-stage solution $\boldsymbol{u}_{n,2}$ satisfy (3.10) and (3.11), respectively.

For the final solution $\boldsymbol{u}^{n+1}$, we infer that

$$\begin{aligned}
&E(\boldsymbol{u}^{n+1})-E(\boldsymbol{u}_{n,2})\leq-\left\langle \boldsymbol{u}^{n+1}-\boldsymbol{u}_{n,2},L_\kappa\boldsymbol{u}^{n+1}+N_\kappa(\boldsymbol{u}_{n,2})\right\rangle_H\\
&=-\left\langle \boldsymbol{u}^{n+1}-\boldsymbol{u}_{n,2},L_\kappa\boldsymbol{u}^{n+1}-L_\kappa\boldsymbol{u}_{n,2}+(\tau\varphi_2)^{-1}(\boldsymbol{u}^{n+1}-\boldsymbol{u}_{n,2})+L_\kappa\boldsymbol{u}_{n,2}+N_\kappa(\boldsymbol{u}_{n,1})\right\rangle_H\\
&=\langle \boldsymbol{u}^{n+1}-\boldsymbol{u}_{n,2},\Delta_2(\boldsymbol{u}^{n+1}-\boldsymbol{u}_{n,2})\rangle_h+\langle \boldsymbol{u}^{n+1}-\boldsymbol{u}_{n,2},\Delta_1(\boldsymbol{u}_{n,1}-\boldsymbol{u}^n)\rangle_h\\
&+\langle \boldsymbol{u}^{n+1}-\boldsymbol{u}_{n,2},\Delta_2(\boldsymbol{u}_{n,2}-\boldsymbol{u}_{n,1})\rangle_h.
\end{aligned}\tag{3.13}$$

Adding (3.10) and (3.11) to (3.13) yields

$$\begin{aligned}
E(\boldsymbol{u}^{n+1})-E(\boldsymbol{u}^n)\leq&\underbrace{\langle \boldsymbol{u}_{n,1}-\boldsymbol{u}^n,\Delta_1(\boldsymbol{u}_{n,1}-\boldsymbol{u}^n)\rangle_h}_{A}+\underbrace{\langle \boldsymbol{u}_{n,2}-\boldsymbol{u}_{n,1},\Delta_2(\boldsymbol{u}_{n,2}-\boldsymbol{u}_{n,1})\rangle_h}_{B}\\
&+\underbrace{\langle \boldsymbol{u}^{n+1}-\boldsymbol{u}_{n,2},\Delta_2(\boldsymbol{u}^{n+1}-\boldsymbol{u}_{n,2})\rangle_h}_{C}+\underbrace{\langle \boldsymbol{u}_{n,2}-\boldsymbol{u}_{n,1},\Delta_1(\boldsymbol{u}_{n,1}-\boldsymbol{u}^n)\rangle_h}_{D}\\
&+\underbrace{\langle \boldsymbol{u}^{n+1}-\boldsymbol{u}_{n,2},\Delta_1(\boldsymbol{u}_{n,1}-\boldsymbol{u}^n)\rangle_h}_{E}+\underbrace{\langle \boldsymbol{u}^{n+1}-\boldsymbol{u}_{n,2},\Delta_2(\boldsymbol{u}_{n,2}-\boldsymbol{u}_{n,1})\rangle_h}_{F},
\end{aligned}$$

where

$$\begin{aligned}
B=&\underbrace{\frac{1}{2}\langle \boldsymbol{u}_{n,2}-\boldsymbol{u}_{n,1},\Delta_1(\boldsymbol{u}_{n,2}-\boldsymbol{u}_{n,1})\rangle_h}_{B_1}+\underbrace{\frac{1}{2}\langle \boldsymbol{u}_{n,2}-\boldsymbol{u}_{n,1},\Delta_2(\boldsymbol{u}_{n,2}-\boldsymbol{u}_{n,1})\rangle_h}_{B_2}\\
&+\underbrace{\frac{1}{2}\langle \boldsymbol{u}_{n,2}-\boldsymbol{u}_{n,1},(\Delta_2-\Delta_1)(\boldsymbol{u}_{n,2}-\boldsymbol{u}_{n,1})\rangle_h}_{B_3},
\end{aligned}$$

and

$$\begin{aligned}
C=&\underbrace{\frac{1}{2}\langle \boldsymbol{u}^{n+1}-\boldsymbol{u}_{n,2},\Delta_1(\boldsymbol{u}^{n+1}-\boldsymbol{u}_{n,2})\rangle_h}_{C_1}+\underbrace{\frac{1}{2}\langle \boldsymbol{u}^{n+1}-\boldsymbol{u}_{n,2},\Delta_2(\boldsymbol{u}^{n+1}-\boldsymbol{u}_{n,2})\rangle_h}_{C_2}\\
&+\underbrace{\frac{1}{2}\langle \boldsymbol{u}^{n+1}-\boldsymbol{u}_{n,2},(\Delta_2-\Delta_1)(\boldsymbol{u}^{n+1}-\boldsymbol{u}_{n,2})\rangle_h}_{C_3}.
\end{aligned}$$

Since $\Delta_2-\Delta_1$ is negative definite, it holds that $B_3\leq 0$ and $C_3\leq 0$.

Note that

$$\frac{1}{2}D+B_1=\frac{1}{2}\langle \boldsymbol{u}_{n,2}-\boldsymbol{u}_{n,1},\Delta_1(\boldsymbol{u}_{n,2}-\boldsymbol{u}^n)\rangle_h,\qquad \frac{1}{2}(D+A)=\frac{1}{2}\langle \boldsymbol{u}_{n,2}-\boldsymbol{u}^n,\Delta_1(\boldsymbol{u}_{n,1}-\boldsymbol{u}^n)\rangle_h,$$
$$\frac{1}{2}F+B_2=\frac{1}{2}\langle \boldsymbol{u}^{n+1}-\boldsymbol{u}_{n,1},\Delta_2(\boldsymbol{u}_{n,2}-\boldsymbol{u}_{n,1})\rangle_h,\quad \frac{1}{2}F+C_2=\frac{1}{2}\langle \boldsymbol{u}^{n+1}-\boldsymbol{u}_{n,2},\Delta_2(\boldsymbol{u}^{n+1}-\boldsymbol{u}_{n,1})\rangle_h,$$
$$\frac{1}{2}E+C_1=\frac{1}{2}\langle \boldsymbol{u}^{n+1}-\boldsymbol{u}_{n,2},\Delta_1(\boldsymbol{u}^{n+1}-\boldsymbol{u}_{n,2}+\boldsymbol{u}_{n,1}-\boldsymbol{u}^n)\rangle_h,$$
$$\frac{1}{2}(E+A)=\frac{1}{2}\langle \boldsymbol{u}^{n+1}-\boldsymbol{u}_{n,2}+\boldsymbol{u}_{n,1}-\boldsymbol{u}^n,\Delta_1(\boldsymbol{u}_{n,1}-\boldsymbol{u}^n)\rangle_h.$$

Then, applying the symmetry and negative definiteness of $\Delta_1$ and $\Delta_2$, we obtain

$$D+B_1+\frac{1}{2}A=\frac{1}{2}\langle \boldsymbol{u}_{n,2}-\boldsymbol{u}^n,\Delta_1(\boldsymbol{u}_{n,2}-\boldsymbol{u}^n)\rangle_h\le 0,$$
$$F+B_2+C_2=\frac{1}{2}\langle \boldsymbol{u}^{n+1}-\boldsymbol{u}_{n,1},\Delta_2(\boldsymbol{u}^{n+1}-\boldsymbol{u}_{n,1})\rangle_h\le 0,$$
$$E+C_1+\frac{1}{2}A=\frac{1}{2}\langle \boldsymbol{u}^{n+1}-\boldsymbol{u}_{n,2}+\boldsymbol{u}_{n,1}-\boldsymbol{u}^n,\Delta_1(\boldsymbol{u}^{n+1}-\boldsymbol{u}_{n,2}+\boldsymbol{u}_{n,1}-\boldsymbol{u}^n)\rangle_h\le 0.$$

Finally, we obtain

$$E(\boldsymbol{u}^{n+1})-E(\boldsymbol{u}^n)\le (D+B_1+\frac{1}{2}A)+(E+C_1+\frac{1}{2}A)+(F+B_2+C_2)+B_3+C_3\le 0.$$

The proof is completed. □

## 4. Error estimate

Thanks to the uniform $l^\infty$ boundedness of the numerical solutions ensured by the MPP property of the proposed schemes, in this section, we analyze the error estimate of the fully discrete stabilized ETDRK schemes (3.5). We define the operator $\mathcal{I}_h$ to limit a function $u:\Omega\to\mathbb{R}$ on the mesh $\Omega_h$ such that

$$(\mathcal{I}_h u)_i=u(x_i),\quad \forall u\in C(\bar{\Omega}).$$

Denote by $u_e(\mathbf{x},t)$ the exact solution of (1.1) and we obtain the space-discrete equation for $u_e(t)$ of the problem (1.1):

$$(I-\nu\Delta_h)\frac{\mathrm{d}\mathcal{I}_h u_e(t)}{\mathrm{d}t}+\epsilon^2\Delta_h^2\mathcal{I}_h u_e(t)=\Delta_h f(\mathcal{I}_h u_e(t))+R_{h_1},\tag{4.1}$$

while using the second-order central difference method yields the following ODE:

$$(I-\nu\Delta_h)\frac{\mathrm{d}\boldsymbol{u}(t)}{\mathrm{d}t}+\epsilon^2\Delta_h^2\boldsymbol{u}(t)=\Delta_h f(\boldsymbol{u}(t)).\tag{4.2}$$

By discerning between (4.1) and (4.2), it is straightforward to derive the expansion of the truncated error $R_{h_1}$:

$$\begin{aligned}R_{h_1}&=\epsilon^2\Delta_h^2\mathcal{I}_h u_e(t)-\epsilon^2\Delta_h^2\boldsymbol{u}+\Delta_h f(\boldsymbol{u}(t))-\Delta_h f(\mathcal{I}_h u_e(t))+\nu\Delta_h\frac{\mathrm{d}\boldsymbol{u}(t)}{\mathrm{d}t}-\nu\Delta_h\frac{\mathrm{d}\mathcal{I}_h u_e(t)}{\mathrm{d}t}\\&=\mathcal{O}(h^2).\end{aligned}$$

By adding and subtracting additional terms $\frac{\epsilon^2}{\nu}\Delta_h\mathcal{I}_h u_e$ and $\kappa\mathcal{I}_h u_e$, we apply an equivalent transformation once more to (4.1); that is,

$$\begin{aligned}\frac{\mathrm{d}\mathcal{I}_h u_e}{\mathrm{d}t}&=(I-\nu\Delta_h)^{-1}\left[-\epsilon^2\Delta_h^2\mathcal{I}_h u_e+\Delta_h f(\mathcal{I}_h u_e)+R_{h_1}\right]\\&=(I-\nu\Delta_h)^{-1}\left[\left(\frac{\epsilon^2}{\nu}I-\epsilon^2\Delta_h\right)\Delta_h\mathcal{I}_h u_e+\Delta_h\left(f(\mathcal{I}_h u_e)-\frac{\epsilon^2}{\nu}\mathcal{I}_h u_e\right)+R_{h_1}\right]\\&=\frac{\epsilon^2}{\nu}\Delta_h\mathcal{I}_h-\kappa\mathcal{I}_h u_e+\frac{1}{\nu}\left[(I-\nu\Delta_h)^{-1}-I\right]\left(f(\mathcal{I}_h u_e)-\frac{\epsilon^2}{\nu}\mathcal{I}_h u_e\right)+\kappa\mathcal{I}_h u_e+(I-\nu\Delta_h)^{-1}R_{h_1}\\&=:L_\kappa\mathcal{I}_h u_e+N_\kappa(\mathcal{I}_h u_e)+R_h.\end{aligned}$$

A straightforward derivation demonstrates that the truncated error in the space-discrete domain is of second order:

$$\|R_h\|_{l^\infty} \le \|(I-\nu\Delta_h)^{-1}\|_\infty \|R_{h_1}\|_{l^\infty} \le C_1 h^2,$$

where the positive constant $C_1$ is independent of $h$. In particular, it is important to highlight that the notations $C, C_1$, and $C_2$ used in this section bear no relation to the same ones mentioned in Section 3. The main convergence result is now presented.

**Theorem 4.1.** *Assume that the viscous Cahn–Hilliard equation (2.1) has an exact solution $u(t) \in C^{p+1}(0,T;C^6(\bar{\Omega}))$ and $\boldsymbol{u}^n$ is computed by the fully discrete ETDRK schemes given by (3.5), which are equipped with the Butcher-like tableaus in (3.4). If the initial values satisfy the maximum principle in Theorem 2.1, we have the error estimate,*

$$\|\boldsymbol{u}^n - \mathcal{I}_h u_e(t_n)\|_{l^\infty} \le C(e^{3C_0\kappa s t_n}-1)(h^2+\tau^p), \quad p=1,2$$

*for any $h>0$ and $\tau>0$, where the constant $C$ depends on the $C^{p+1}(0,T;C^6(\bar{\Omega}))$-norm of $u$, $s$, $\kappa$, $t_n$, but is independent of $h$ and $\tau$.*

**Proof.** By using the fully discrete stabilized ETDRK schemes (3.5), we introduce reference functions [71] $U_{n,i}$ for $0 \le i \le s$ with $U_{n,0} = u(\mathbf{x}, t_n)$ and $U_{n,s} = u(\mathbf{x}, t_n+\tau)$ satisfying

$$\begin{aligned} U_{n,i} &= \varphi_0(c_i\tau L_\kappa)U_{n,0} + \tau\sum_{j=0}^{i-1} a_{i,j}(\tau L_\kappa)\left[N_\kappa(U_{n,j}) + R_h(U_{n,j})\right], \quad i=1,\cdots,s-1,\\ U_{n,s} &= \varphi_0(\tau L_\kappa)U_{n,0} + \tau\sum_{j=0}^{s-1} a_{s,j}(\tau L_\kappa)\left[N_\kappa(U_{n,j}) + R_h(U_{n,j})\right] + R_\tau^n. \end{aligned} \tag{4.3}$$

Let $e_n = U_{n,0} - \boldsymbol{u}^n$ and $e_{n,i} = U_{n,i} - \boldsymbol{u}_{n,i}$ for $0 \le i \le s$. Subtracting (3.5) from (4.3) yields

$$\begin{aligned} e_{n,i} &= \varphi_0(c_i\tau L_\kappa)e^n + \tau\sum_{j=0}^{i-1} a_{i,j}(\tau L_\kappa)\left[N_\kappa(U_{n,j}) - N_\kappa(\boldsymbol{u}_{n,j}) + R_h(U_{n,j})\right], \quad i=1,\cdots,s-1,\\ e_{n,s} &= \varphi_0(\tau L_\kappa)e^n + \tau\sum_{j=0}^{s-1} a_{s,j}(\tau L_\kappa)\left[N_\kappa(U_{n,j}) - N_\kappa(\boldsymbol{u}_{n,j}) + R_h(U_{n,j})\right] + R_\tau^n. \end{aligned} \tag{4.4}$$

$R_\tau^n$ is the truncated temporal error, which satisfies

$$\max_{0\le n\le \lfloor T/\tau\rfloor -1} \sup \|R_\tau^n\|_{l^\infty} \le C_2\tau^{p+1}, \tag{4.5}$$

where the constant $C_2$ depends on the $C^{p+1}(0,T;C^6(\bar{\Omega}))$-norm of $u$, $s$, $\kappa$, but is independent of $\tau$. Applying Lemmas 3.2–3.5 and using the MPP property of the proposed schemes, we derive

$$\begin{aligned} \|e_{n,i}\|_{l^\infty} &\le \|\varphi_0(c_i\tau L_\kappa)\|_\infty \|e^n\|_{l^\infty} + \tau\sum_{j=0}^{i-1}\|a_{i,j}(\tau L_\kappa)\|_\infty \|N_\kappa(U_{n,j}) - N_\kappa(\boldsymbol{u}_{n,j})\|_{l^\infty}\\ &\quad + \tau\|\sum_{j=0}^{i-1} a_{i,j}(\tau L_\kappa)R_h(U_{n,j})\|_{l^\infty}\\ &\le \underbrace{\varphi_0(-c_i\tau\kappa)}_{<1}\|e^n\|_{l^\infty} + 3c_i\tau\kappa\,\underbrace{\varphi_1(-c_i\tau\kappa)}_{<1}\sum_{j=0}^{i-1}\|e_{n,j}\|_{l^\infty} + c_i\tau\varphi_1(-c_i\tau\kappa)C_1h^2\\ &\le \|e^n\|_{l^\infty} + 3C_0\tau\kappa\sum_{j=0}^{i-1}\|e_{n,j}\|_{l^\infty} + C_1C_0h^2\tau, \end{aligned} \tag{4.6}$$

where $C_0$ denotes the maximum value of $c_i$, i.e., $C_0 = \max\{c_0,\ldots,c_{s-1},c_s\}$.

By induction, we obtain

$$\|e_{n,i}\|_{l^\infty} \le (1+3C_0\tau\kappa)^i\|e^n\|_{l^\infty} + (1+3C_0\tau\kappa)^{i-1}C_1C_0h^2\tau, \quad i=1,\cdots,s-1.$$

Continuing in this fashion and using the truncated temporal error (4.5), it holds that

**Table 1**
Selections of the maximum bound $\beta$ and stabilizing constant $\kappa$ for two different potential functions ($\theta = 0.8$ and $\theta_c = 1.6$ for Flory-Huggins potential).

| Parameters | | Ginzburg–Landau polynomial potential | | Flory–Huggins logarithmic potential | |
|---|---|---|---|---|---|
| $\epsilon$ | $\nu$ | $\beta$ | $\kappa$ | $\beta$ | $\kappa$ |
| 0.01 | 1 | 1.15475827 | 3.00 | 0.98678947 | 28.88 |

$$
\begin{aligned}
\|e_{n,s}\|_{l^\infty} &\le \|\varphi_0(\tau L_\kappa)\|_\infty \|e^n\|_{l^\infty} + \tau \sum_{j=0}^{s-1} \|a_{s,j}(\tau L_\kappa)\|_\infty \|N_\kappa(U_{n,j}) - N_\kappa(\boldsymbol{u}_{n,j})\|_{l^\infty} \\
&+ \tau \sum_{j=0}^{s-1} \|a_{s,j}(\tau L_\kappa)\|_\infty \|R_h(U_{n,j})\|_{l^\infty} + \|R_\tau^n\|_{l^\infty} \\
&\le \varphi_0(-\tau\kappa)\|e^n\|_{l^\infty} + 3c_s\tau\kappa \underbrace{\varphi_1(-c_s\tau\kappa)}_{<1} \sum_{j=0}^{s-1} \|e_{n,j}\|_{l^\infty} + c_s\tau\varphi_1(-c_s\tau\kappa)C_1h^2 + \|R_\tau^n\|_{l^\infty} \\
&\le \|e^n\|_{l^\infty} + 3C_0\tau\kappa \sum_{j=0}^{s-1} \|e_{n,j}\|_{l^\infty} + C_1C_0h^2\tau + C_2\tau^{p+1} \\
&\le (1+3C_0\tau\kappa)^s \|e^n\|_{l^\infty} + (1+3C_0\tau\kappa)^{s-1} C_1C_0h^2\tau + C_2\tau^{p+1}.
\end{aligned}
\tag{4.7}
$$

Setting $\|e^0\|_{l^\infty} = 0$, by induction, we obtain

$$
\begin{aligned}
\|e^n\|_{l^\infty} &\le (1+3C_0\tau\kappa)^{sn}\|e^0\|_{l^\infty} + \sum_{k=1}^{n}(1+3C_0\tau\kappa)^{ks}\frac{C_1C_0h^2\tau}{1+3C_0\tau\kappa} + \sum_{k=0}^{n-1}(1+3C_0\tau\kappa)^{ks}C_2\tau^{p+1} \\
&\le \frac{(1+3C_0\tau\kappa)^s[(1+3C_0\tau\kappa)^{sn}-1]}{3C_0\tau\kappa s} \cdot \frac{C_1C_0h^2\tau}{1+3C_0\tau\kappa} + [(1+3C_0\tau\kappa)^{ns}-1]\frac{C_2\tau^{p+1}}{3C_0\tau\kappa s} \\
&= \frac{(1+3C_0\tau\kappa)^{sn}-1}{3C_0\kappa s}[(1+3C_0\tau\kappa)^{s-1}C_1C_0h^2 + C_2\tau^p] \\
&< \frac{(1+3C_0\tau\kappa)^{sn}-1}{3C_0\kappa s}[(1+3C_0\kappa t_n)^{s-1}C_1C_0h^2 + C_2\tau^p] \\
&= C(e^{3C_0\kappa s t_n}-1)(h^2+\tau^p),
\end{aligned}
\tag{4.8}
$$

where $n\tau = t_n$ and $C = \frac{1}{3C_0\kappa s}\max\{(1+3C_0\kappa t_n)^{s-1}C_1C_0, C_2\}$. This completes the proof. □

## 5. Numerical results

In this section, we first tested the temporal and spatial convergence orders and compared the errors between different second-order ETDRK schemes. We then simulated the coarsening dynamics of the viscous Cahn–Hilliard equation in 2D and 3D cases, and we showed that the three properties of the viscous Cahn–Hilliard equation were preserved by several numerical examples. Finally, we compared and analyzed the computational efficiency among second-order ETDRK schemes. When adopting ETDRK schemes, we computed the products of the matrix exponential with vectors by the fast Fourier transform to accelerate the computations [57]. Please note that the parameter $c_1$ in the ETD II-IV schemes was set to 1 for numerical convenience. It is important to mention that except for Equation (5.3), which was under homogeneous Neumann boundary conditions, all other experiments were conducted under periodic boundary conditions. Below, we gave the results about the specific selections of the stabilizing constant $\kappa$ and the maximum bound $\beta$; that is,

(1) for the Ginzburg–Landau polynomial potential (1.2), $\beta = \sqrt{\frac{4}{3}(1+\frac{\epsilon^2}{\nu})}$, $\kappa = \frac{3\beta^2-1-\epsilon^2/\nu}{\nu}$;
(2) for the Flory–Huggins logarithmic potential (1.3), $\beta = M^+$, $\kappa = \frac{1}{\nu}(\frac{\theta}{1-\beta^2} - \theta_c - \frac{\epsilon^2}{\nu})$, where $M^+$ is the positive root of $f_1\left(-\sqrt{1-\frac{\theta}{\theta_c+\frac{\epsilon^2}{\nu}}}\right)$.

According to these results, we listed the values of $\kappa$ and $\beta$ that would be utilized later in Table 1.

**Table 2**
Errors and convergence rates of the ETD I scheme.

| $\tau$ | $\kappa = 3$ | | $\kappa = 4$ | | $\kappa = 10$ | |
|---|---|---|---|---|---|---|
| | $l^\infty$ error | Order | $l^\infty$ error | Order | $l^\infty$ error | Order |
| $2^{-1}$ | 3.5463E−1 | – | 3.9504E−1 | – | 4.9762E−1 | – |
| $2^{-2}$ | 2.3842E−1 | 0.57 | 2.7923E−1 | 0.50 | 4.1874E−1 | 0.25 |
| $2^{-3}$ | 1.4144E−1 | 0.75 | 1.7188E−1 | 0.70 | 3.0468E−1 | 0.46 |
| $2^{-4}$ | 7.7342E−2 | 0.87 | 9.6012E−2 | 0.84 | 1.9133E−1 | 0.67 |
| $2^{-5}$ | 4.0443E−2 | 0.93 | 5.0834E−2 | 0.92 | 1.0812E−1 | 0.82 |
| $2^{-6}$ | 2.0685E−2 | 0.97 | 2.6119E−2 | 0.96 | 5.7528E−2 | 0.91 |
| $2^{-7}$ | 1.0460E−2 | 0.98 | 1.3245E−2 | 0.98 | 2.9669E−2 | 0.96 |
| $2^{-8}$ | 5.2980E−3 | 0.99 | 6.6690E−3 | 0.99 | 1.5065E−2 | 0.98 |

**Table 3**
Errors and convergence rates of the ETD II scheme.

| $\tau$ | $\kappa = 3$ | | $\kappa = 4$ | | $\kappa = 10$ | |
|---|---|---|---|---|---|---|
| | $l^\infty$ error | Order | $l^\infty$ error | Order | $l^\infty$ error | Order |
| $2^{-1}$ | 1.9743E−1 | – | 2.5188E−1 | – | 4.2329E−1 | – |
| $2^{-2}$ | 8.2302E−2 | 1.26 | 1.1629E−1 | 1.12 | 2.8754E−1 | 1.26 |
| $2^{-3}$ | 2.7482E−2 | 1.59 | 4.1260E−2 | 1.49 | 1.4144E−1 | 1.59 |
| $2^{-4}$ | 8.0154E−3 | 1.78 | 1.2439E−2 | 1.73 | 5.2242E−2 | 1.78 |
| $2^{-5}$ | 2.2330E−3 | 1.89 | 3.4268E−3 | 1.86 | 1.6094E−2 | 1.89 |
| $2^{-6}$ | 5.5933E−4 | 1.94 | 9.0008E−4 | 1.93 | 4.4831E−3 | 1.94 |
| $2^{-7}$ | 1.4624E−4 | 1.97 | 2.3071E−4 | 1.96 | 1.1184E−3 | 1.97 |
| $2^{-8}$ | 3.6011E−5 | 1.99 | 5.8405E−5 | 1.98 | 3.0442E−4 | 1.99 |

**Table 4**
Errors and convergence rates of the ETD III scheme.

| $\tau$ | $\kappa = 3$ | | $\kappa = 4$ | | $\kappa = 10$ | |
|---|---|---|---|---|---|---|
| | $l^\infty$ error | Order | $l^\infty$ error | Order | $l^\infty$ error | Order |
| $2^{-1}$ | 2.2878E−1 | – | 2.8712E−1 | – | 4.5233E−1 | – |
| $2^{-2}$ | 9.9834E−2 | 1.20 | 1.3989E−1 | 1.04 | 3.2537E−1 | 1.26 |
| $2^{-3}$ | 3.4153E−2 | 1.55 | 5.1393E−2 | 1.44 | 1.7020E−1 | 1.59 |
| $2^{-4}$ | 1.0132E−2 | 1.76 | 9.6012E−2 | 1.70 | 6.5577E−2 | 1.78 |
| $2^{-5}$ | 2.7454E−3 | 1.88 | 1.5793E−2 | 1.85 | 2.0683E−2 | 1.89 |
| $2^{-6}$ | 7.1550E−4 | 1.94 | 4.3947E−3 | 1.92 | 5.8338E−3 | 1.94 |
| $2^{-7}$ | 1.8283E−4 | 1.97 | 2.9820E−4 | 1.96 | 1.5510E−3 | 1.97 |
| $2^{-8}$ | 4.6207E−5 | 1.98 | 7.5590E−5 | 1.98 | 3.9998E−4 | 1.99 |

### 5.1. Convergence tests

We started by verifying numerically that our schemes are first- and second-order accurate in time. Let us consider the viscous Cahn–Hilliard equation (2.1) with the Ginzburg–Landau polynomial potential (1.2) in the 1D case. The initial condition was given by

$$u_0 = \sin(x), \quad x \in \Omega. \tag{5.1}$$

The parameters were chosen as follows: $\Omega = (0, 2\pi)$, $T = 2$, $\epsilon = 0.01$, $\kappa = 3, 4, 10$, and $\nu = 1$. To quantify the errors, we first set a large spatial grid number $N = 2^{12}$ and a fine time-step size $\tau_{\text{ref}} = 2^{-14}$ such that the error from the spatial and temporal discretization was negligible. Then, the reference solution $\boldsymbol{u}_{ref}$ was produced by the ETD II scheme. We computed the numerical solutions with time-step sizes $\tau_k = 2^{-k}$, $k = 1, 2, \ldots, 8$.

Tables 2-5 listed the discrete $l^\infty$ errors and corresponding convergence rates of the ETD I-IV schemes. The convergence rates were clearly of the first or second order, and it was easily observed that the errors of the ETD schemes became larger with larger $\kappa$ while the convergence rates were independent on the value of $\kappa$, which confirmed the theoretical results of the numerical analysis in Section 4. Furthermore, although all of the three ETD schemes achieved second-order accuracy, the accuracy of the ETD IV scheme was the highest, even an order of magnitude higher than that of the ETD II scheme, which also illustrated that the increase in the stage resulted in the improvement of the accuracy.

**Table 5**
Errors and convergence rates of the ETD IV scheme.

| $\tau$ | $\kappa = 3$ | | $\kappa = 4$ | | $\kappa = 10$ | |
|---|---|---|---|---|---|---|
| | $l^\infty$ error | Order | $l^\infty$ error | Order | $l^\infty$ error | Order |
| $2^{-1}$ | 1.0046E−1 | – | 1.5074E−1 | – | 3.5425E−1 | – |
| $2^{-2}$ | 2.4363E−2 | 2.05 | 4.3476E−2 | 1.79 | 1.8940E−1 | 0.90 |
| $2^{-3}$ | 3.9764E−3 | 2.63 | 8.2089E−3 | 2.41 | 6.1676E−2 | 1.62 |
| $2^{-4}$ | 4.7448E−4 | 3.05 | 1.1120E−3 | 2.88 | 1.3129E−2 | 2.23 |
| $2^{-5}$ | 6.3680E−5 | 2.90 | 1.2607E−4 | 3.14 | 2.0803E−3 | 2.66 |
| $2^{-6}$ | 2.3239E−5 | 1.45 | 1.8615E−5 | 2.76 | 2.6456E−4 | 2.98 |
| $2^{-7}$ | 7.7844E−6 | 1.58 | 8.4159E−6 | 1.15 | 2.8260E−5 | 3.23 |
| $2^{-8}$ | 2.2127E−6 | 1.81 | 2.6177E−6 | 1.68 | 3.4274E−6 | 3.04 |

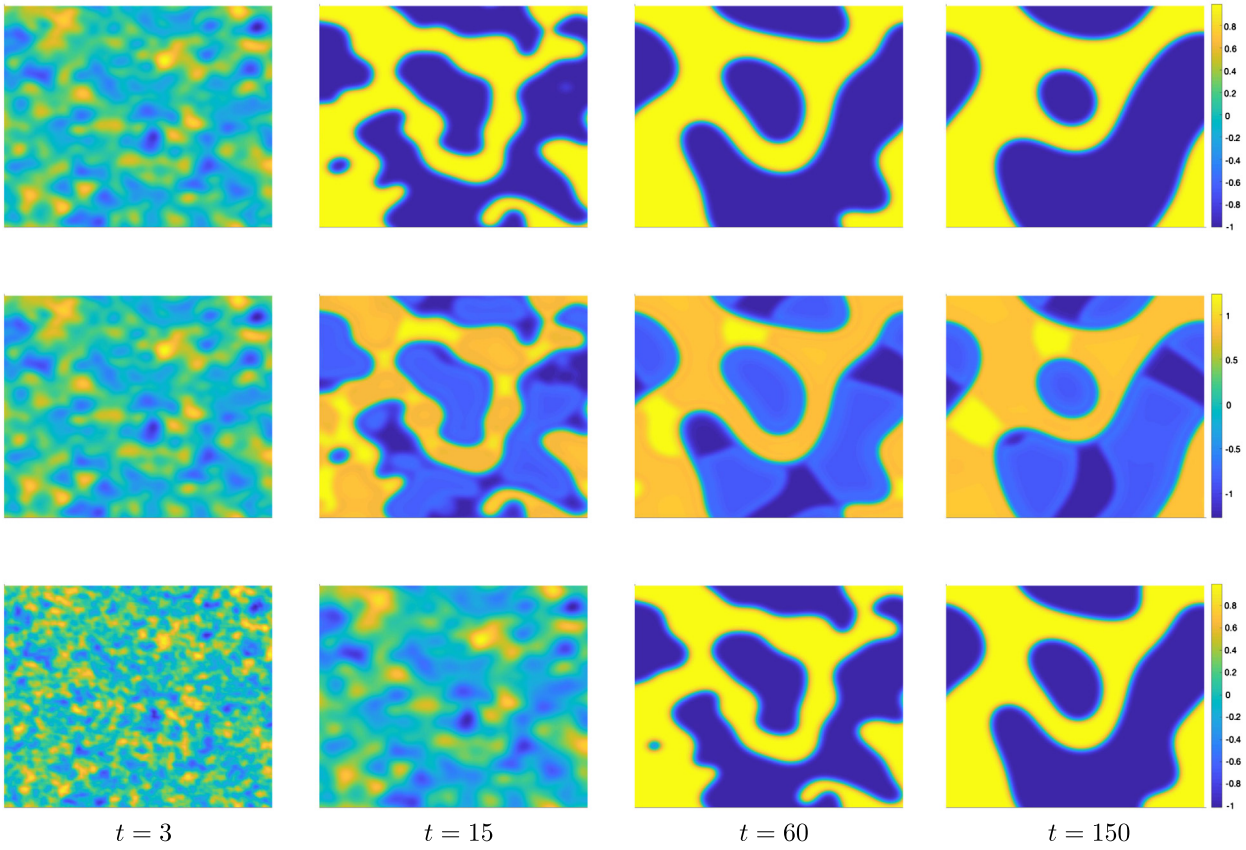


**Fig. 1.** Evolution of 2D random numerical solutions at $t = 3,\ 15,\ 60$, and 150 computed by the ETD IV scheme with different time-step sizes. From top to bottom: $\tau = 0.1$, $\kappa = 3$; $\tau = 1.5$, $\kappa = 0.1$; $\tau = 1.5$, $\kappa = 3$.

### 5.2. Structure-preserving tests

Next, we simulated long-time 2D dynamic coarsening processes governed by the viscous Cahn–Hilliard equation (2.1) and compared the structure-preserving properties between different ETDRK schemes. To demonstrate the stability and robustness of the proposed schemes, we considered initial data that was a random state; that is,

$$u_0 = 0.01 \times \mathbf{rand}(x, y) - 0.05, \quad (x, y) \in \Omega, \tag{5.2}$$

where $\mathbf{rand}(x, y)$ is uniformly distributed in $(0, 1)$. We chose the following parameters: $N = 128^2$, $\nu = 1$, $\epsilon = 0.01$, and $\Omega = (0, 1)^2$. Based on Table 1, we selected $\beta \approx 1.1548$ and $\beta \approx 0.9868$ for the Ginzburg–Landau polynomial potential (1.2) and Flory–Huggins logarithmic potential (1.3), respectively.

For the Ginzburg–Landau polynomial potential, the corresponding stabilizing constant $\kappa$ was set to 3. To demonstrate the unconditionally stability of the proposed schemes, we set $\kappa = 0.1$ as a comparison. Fig. 1 showed the snapshots of the numerical solution at $t = 3,\ 15,\ 60$, and 150 produced by the ETD IV scheme with different time-step sizes $\tau = 0.1$ and 1.5. The corresponding evolution of the energy, supremum norm, and mass error were shown in Fig. 2. From Fig. 1, we

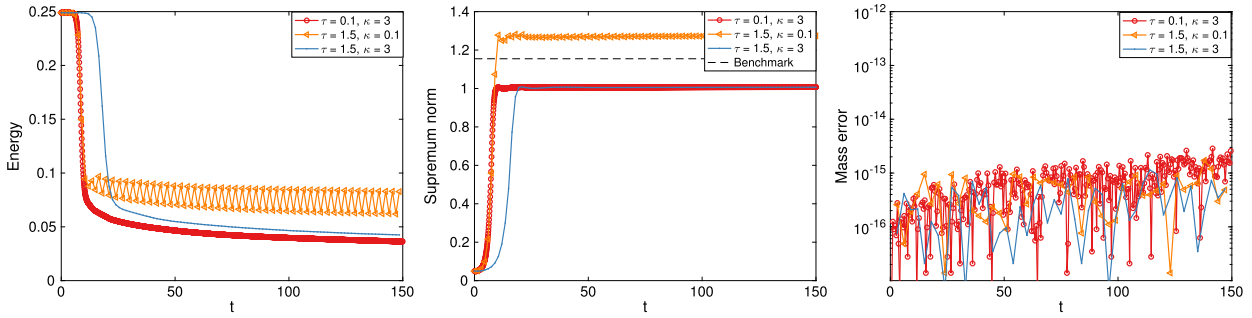


**Fig. 2.** Evolution of energy, supremum norm, and mass error computed by the ETD IV scheme with different time-step sizes and stabilizing constants.

saw that regardless of the time-step size utilized, under the condition $\kappa = 3$, the phases finished separating over a short time, and at large times, they slowly evolved and merged with each other, while under the condition $\kappa = 0.1$ and $\tau = 1$, the oscillations in the solution profile (middle row) appeared. In the whole process, under the condition $\kappa = 3$, the energy always decayed monotonically, the discrete maximum principle was well preserved, and the mass was also conserved, which illustrated the excellent stability of the ETD IV scheme in long-time simulations. However, under the condition $\kappa = 0.1$, it can be observed that although the subfigure in the third row showed that the computed solution conserved the mass to machine accuracy, oscillations appeared in the energy evolution, and the solution broke the maximum bound. In particular, as shown in Fig. 2, as the time-step size increased, the energy dissipation became slower. This phenomenon was also clearly reflected in Fig. 1, which showed that the phase evolution obtained with a larger time-step size was always "later" than the phase obtained with a smaller time-step size. This is unavoidable because of the introduced stabilization term. We notice that this byproduct of stabilization has been observed in Ref. [72,73], etc.

Next, the Flory–Huggins logarithmic potential function was selected, and $\kappa$ was set to 28.88. We used a fixed time-step size ($\tau = 0.1$) and different ETDRK schemes to compute the viscous Cahn–Hilliard equation. Results of these calculations are plotted in Figs. 3 and 4. The numerical simulations of the viscous Cahn–Hilliard equation equipped with the Flory–Huggins logarithmic potential, which is highly nonlinear and singular, again yielded similar evolutionary processes. Moreover, from Fig. 3, we saw that the phase evolution computed by the ETD I scheme was always "later" than the phase computed by the ETD IV scheme, which can also be verified in Fig. 4. From Fig. 4, we also noticed that the order of the numerical scheme corresponding to the energy and maximum bound first reaching the steady-state was ETD IV, ETD II, ETD III, and ETD I, which was also the order of error accuracy. This phenomenon shows that the accuracy of the numerical scheme is strongly correlated with the delayed convergence problem.

To further test the numerical behaviors of the proposed schemes in the 3D case, we considered the following random initial value:

$$u_0 = 0.01 \times \mathbf{rand}(x, y, z) - 0.05, \quad (x, y, z) \in \Omega, \tag{5.3}$$

in which the domain $\Omega$ is $(-1, 1)^3$. The other parameters were chosen as $\epsilon = 0.01$, $N = 128^3$, $\tau = 0.5$, and $\nu = 1$. The test was conducted by using the Ginzburg–Landau polynomial potential and under homogeneous Neumann boundary conditions. We employed the ETD III scheme to compute the solution and presented snapshots at various time points, specifically at $t = 10,\ 20\ ,50,\ 100,\ 200,\ 500$, see Fig. 5. Additionally, we provided the corresponding evolution of energy, supremum norm, and mass error, which are displayed in Fig. 6. Figs. 5 and 6 clearly indicates that when a 3D random initial value is assigned, and in the presence of the restricted homogeneous Neumann boundary condition, the ETD III scheme exhibits the ability to coarsen the phase while preserving the physical structure over an extended period.

Finally, we conducted a performance comparison of different potentials in three dimensions. The corresponding initial value is as follows:

$$\begin{aligned} u_0 = {} & 0.2 \times \tanh\left[100 \times \left(0.2 - |x - 0.15|^{0.8} - |y|^{0.8} - |z - 0.15|^{0.8}\right)\right] \\ & + 0.2 \times \tanh\left[100 \times \left(0.2 - |x + 0.15|^{0.8} - |y|^{0.8} - |z - 0.15|^{0.8}\right)\right] \\ & + 0.2 \times \tanh\left[100 \times \left(0.2 - |x|^{0.8} - |y|^{0.8} - |z + 0.1|^{0.8}\right)\right] + 0.3, \quad (x, y, z) \in \Omega, \end{aligned} \tag{5.4}$$

where the domain $\Omega$ is $(-0.75, 0.75)^3$. The other parameters were chosen as $\epsilon = 0.01$, $N = 128^3$, $\tau = 0.5$, and $\nu = 1$. The stabilizing constants $\kappa$ corresponding to the Ginzburg–Landau polynomial potential and Flory–Huggins logarithmic potential were chosen as 3 and 28.88, respectively.

We used the ETD III scheme to compute the numerical solutions of the viscous Cahn–Hilliard equation and showed the snapshots at $t = 1,\ 10,\ 50$, and 200 in Fig. 7. As time evolved, three independent concave octahedra slowly merged and mixed until finally, they became a hollow sphere with an ellipsoidal inside, marking the shape of the steady-state solution. The computational results that were shown in Fig. 8 again illustrated that whether using the Ginzburg–Landau

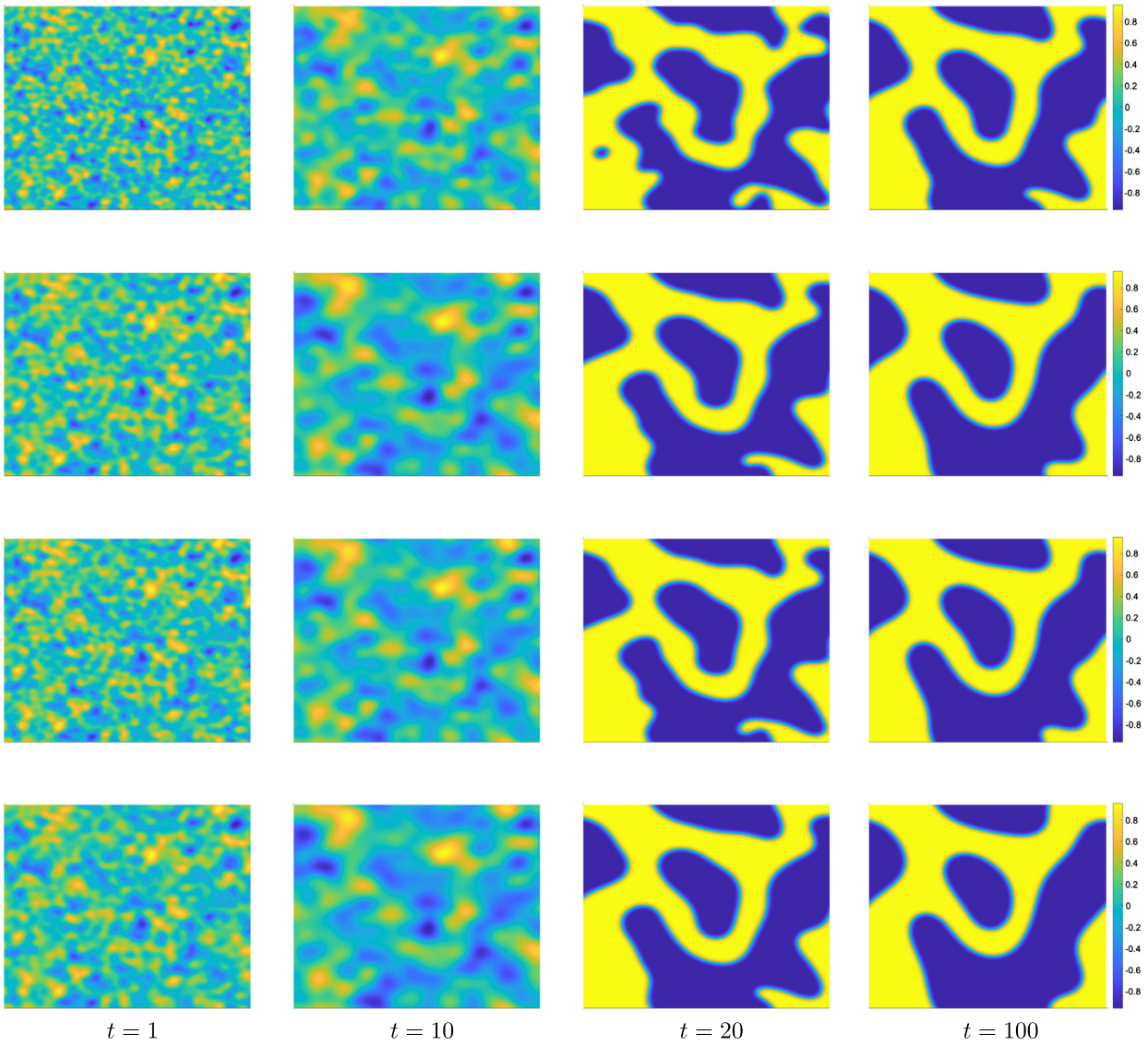


**Fig. 3.** Evolution of 2D random numerical solutions at $t = 1,\ 10,\ 20$, and 100 computed by ETDRK schemes with $\tau = 0.1$. From top to bottom: ETD I, ETD II, ETD III, and ETD IV.

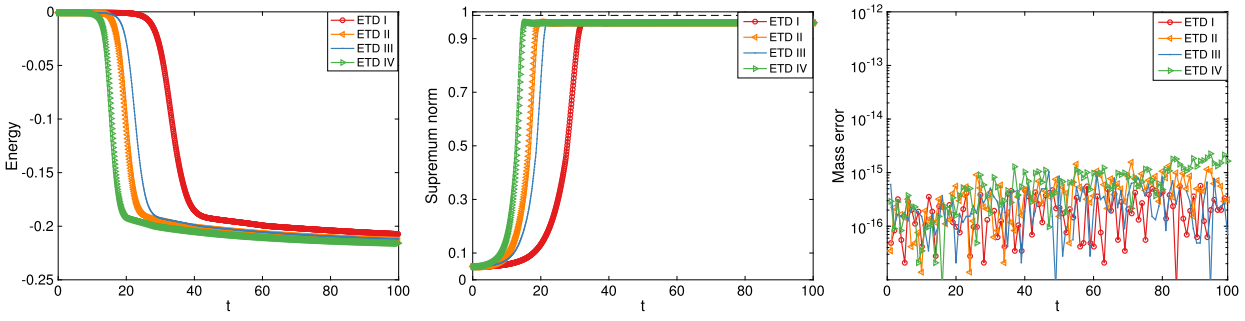


**Fig. 4.** Evolution of energy, supremum norm, and mass error computed by ETDRK schemes with $\tau = 0.1$.

polynomial potential or Flory–Huggins logarithmic potential, the proposed ETDRK schemes (3.5), such as ETD III, always preserve important structure properties of the viscous Cahn–Hillard equation for a long time, even in complex 3D scenarios.

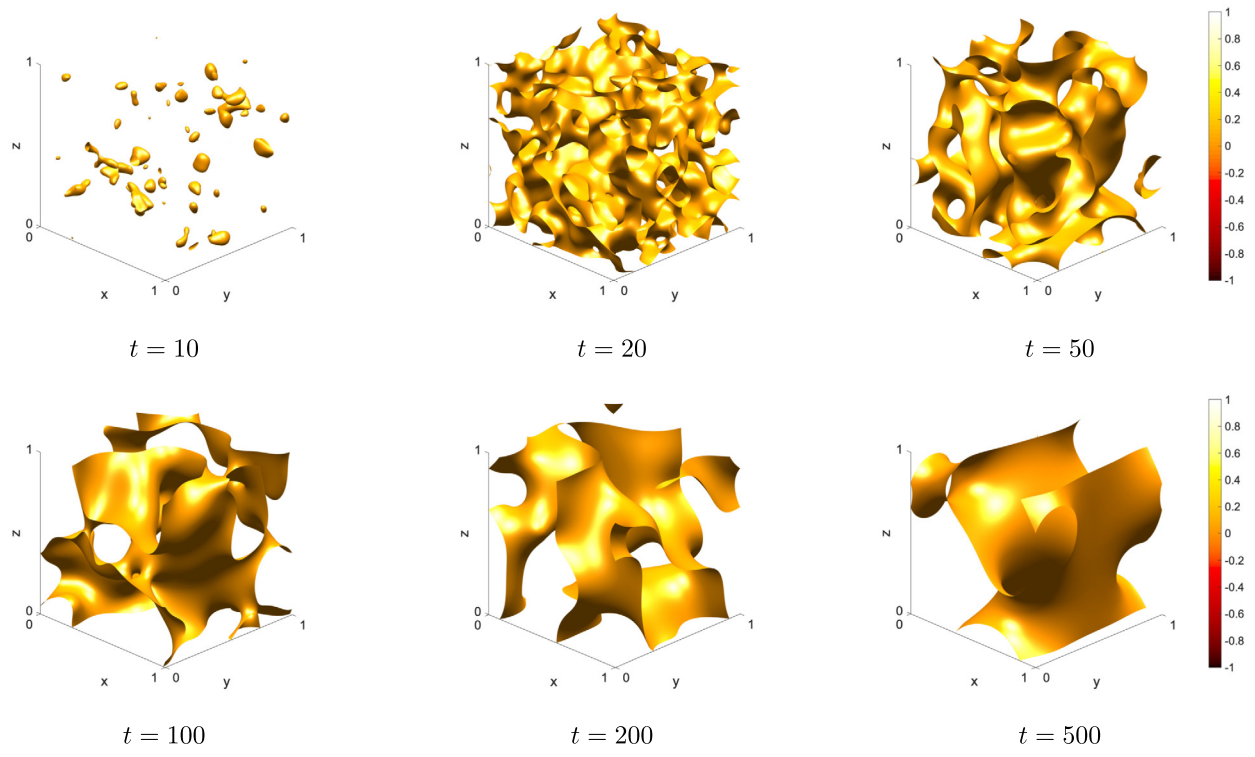


**Fig. 5.** Evolution of 3D random numerical solutions at $t = 10,\ 20,\ 50,\ 100,\ 200$, and 500 computed by the ETD III scheme under homogeneous Neumann boundary conditions.

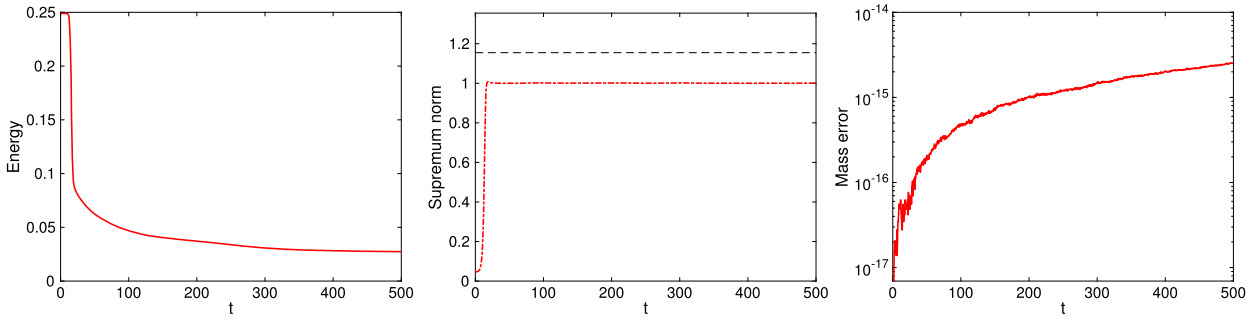


**Fig. 6.** Evolution of energy, supremum norm, and mass error computed by the ETD III scheme under homogeneous Neumann boundary conditions.

### *5.3. Computational efficiency*

We compared the computational costs and accuracy of the proposed second-order ETDRK schemes in 2D and 3D cases. For convenience, Eqs. (5.2) and (5.4) with the Ginzburg–Landau polynomial potential (1.2) were used. For the 2D case, the parameters were selected as follows: $T = 10$, $\epsilon = 0.01$, $\kappa = 3$, $\nu = 1$, $N = 256^2$, and $\tau_{ref} = 2^{-12}$. For the 3D case, the parameters were chosen as follows: $T = 4$, $\epsilon = 0.01$, $\kappa = 3$, $\nu = 1$, $N = 128^3$, and $\tau_{ref} = 2^{-10}$. The numerical solutions with time-step sizes $\tau_k = 2^{-k}$, $k = 1, 2, \cdots, 8$, were computed. With the help of the workstation equipped with an Intel Xeon Gold 6242 2.80-GHz CPU with 128 GB RAM, we obtained the results shown in Fig. 9. In Fig. 9(a), we observed that the curve corresponding to the ETD IV scheme dropped the fastest, while the curve corresponding to the ETD II scheme dropped the slowest, which showed that by combining the two aspects of the computational cost and accuracy, the ETD IV scheme performed the best. These results were shown much more clearly in Fig. 9(b).

## 6. Concluding remarks

In this study, we developed a family of unconditionally stable explicit ETDRK integrators for the viscous Cahn–Hilliard equation. Based on a second-order-in-space reformulation of the viscous Cahn–Hilliard equation, by incorporating the linear stabilization technique, we presented a family of stabilized ETDRK fully discrete schemes (up to second-order both in space

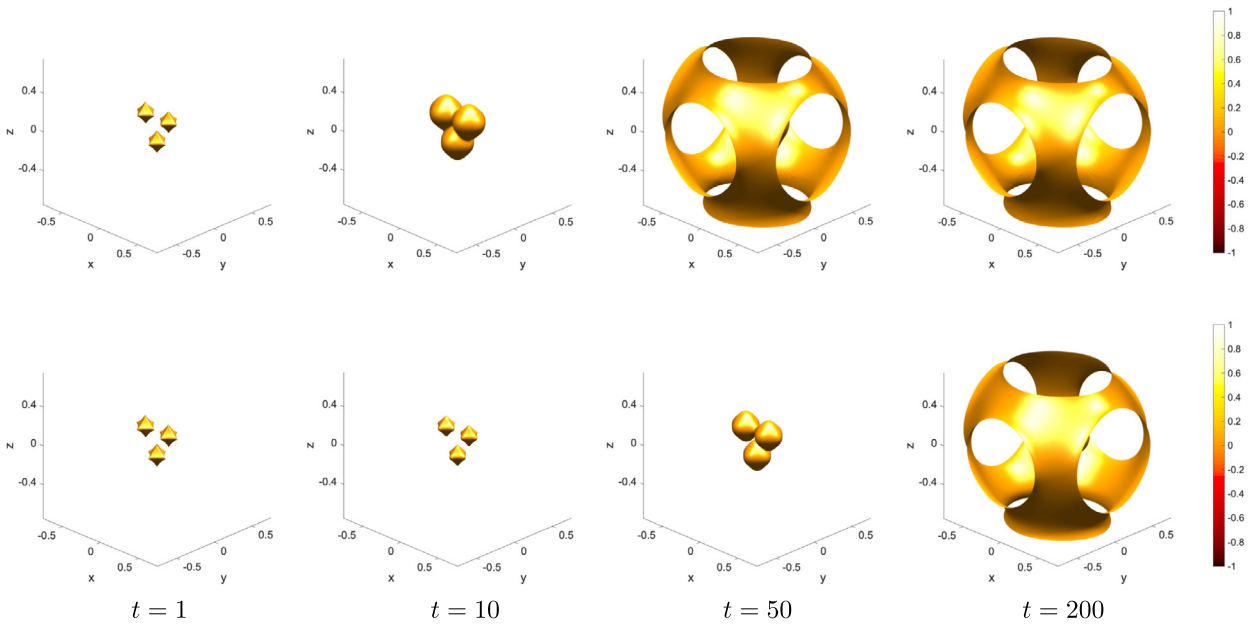


**Fig. 7.** Evolution of 3D numerical solutions at $t = 1,\ 10,\ 50$, and 200 computed by the ETD III scheme. Top: Ginzburg–Landau polynomial potential; bottom: Flory–Huggins logarithmic potential.

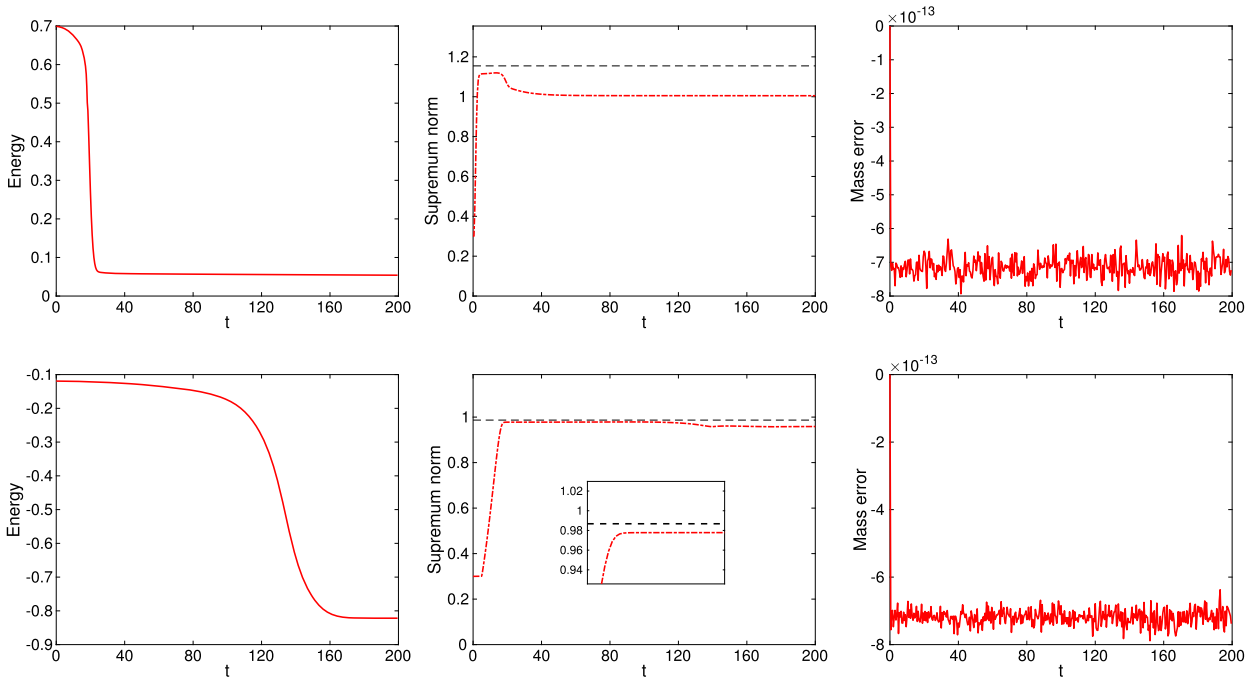


**Fig. 8.** Evolution of energy, supremum norm, and mass error computed by the ETD III scheme. Top: Ginzburg–Landau polynomial potential with $\kappa = 4$; bottom: Flory–Huggins logarithmic potential with $\kappa = 30$.

and time) and provided unified approaches to prove the preservation of the maximum principle and conservation of the mass. In particular, we proved that the stabilized ETDRK ($c_1 = 1$) schemes unconditionally preserve the energy dissipation law for the viscous Cahn–Hilliard equation. Then, we presented a rigorous convergence analysis for fully discrete ETDRK schemes. Numerical experiments demonstrated the ability of the proposed numerical schemes to solve the viscous Cahn–Hilliard equations with the required accuracy, preserve the structure properties, and simulate long-time dynamic evolution of physical models.

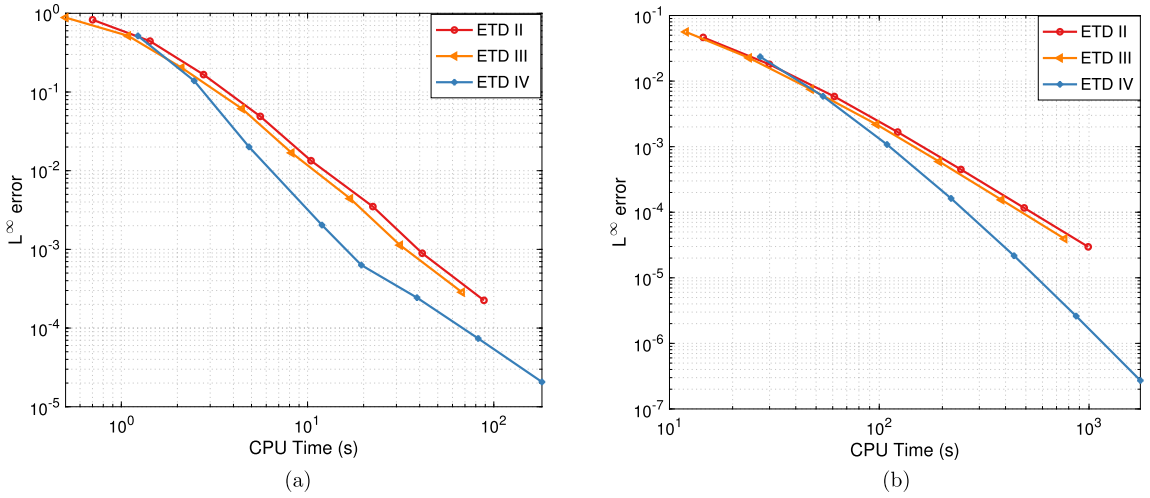


**Fig. 9.** (a) Computational cost and $L^{\infty}$ error plot in 2D case. (b) Computational cost and $L^{\infty}$ error plot in 3D case.

It is worth pointing out that the unified stabilized ETDRK formulation constructed in this study is not limited to the viscous Cahn–Hilliard equation. It can be also applied to other semilinear parabolic equations. Moreover, we notice that there is always a time-delay issue because of the introduction of the stabilization term. We will explore the relaxation framework [61,74] for the stabilization ETDRK schemes in our future studies.

## CRediT authorship contribution statement

**Jingwei Sun:** Conception and design of study, Methodology, Software, Writing – original draft, Writing – review & editing. **Hong Zhang:** Conception and design of study, Writing – review & editing. **Xu Qian:** Conception and design of study, Writing – review & editing. **Songhe Song:** Conception and design of study, Writing – review & editing.

## Declaration of competing interest

No conflict of interest exists.

We wish to confirm that there are no known conflicts of interest associated with this publication and there has been no significant financial support for this work that could have influenced its outcome.

## Data availability

No data was used for the research described in the article.

## Acknowledgements

The authors sincerely thank the anonymous reviewers for their valuable suggestions, which helped improve this manuscript. This research was supported by the National Key R&D Program of China [Grant No. 2020YFA0709803], the National Natural Science Foundation of China [Grant Nos. 12071481, and 12271523], the Natural Science Foundation of Hunan [Grant No. 2021JJ20053], the Defense Science Foundation of China [Grant No. 2021-JCJQ-JJ-0538], the Science and Technology Innovation Program of Hunan Province [Grant Nos. 2021RC3082 and 2022RC1192], and the Research Fund from College of Science, National University of Defense Technology [Grant No. 2023-lxy-fhjj-002].

## References

[1] A. Novick-Cohen, On the viscous Cahn–Hilliard equation, in: Material Instabilities in Continuum Mechanics and Related Mathematical Problems, 1988, pp. 329–342.
[2] J.W. Cahn, J.E. Hilliard, Free energy of a nonuniform system. I. Interfacial free energy, J. Chem. Phys. 28 (2) (1958) 258–267.
[3] A. Bonfoh, M. Grasselli, A. Miranville, Long time behavior of a singular perturbation of the viscous Cahn–Hilliard–Gurtin equation, Math. Methods Appl. Sci. 31 (6) (2008) 695–734.
[4] A. Bonfoh, M. Grasselli, A. Miranville, Inertial manifolds for a singular perturbation of the viscous Cahn–Hilliard–Gurtin equation, Topol. Methods Nonlinear Anal. 35 (1) (2010) 155–185.
[5] L. Cherfils, A. Miranville, Generalized Cahn–Hilliard equations with a logarithmic free energy, Rev. R. Acad. Cienc. Exactas Fís. Nat. 94 (1) (2000) 19–32.
[6] M. Efendiev, H. Gajewski, S. Zelik, The finite dimensional attractor for a 4th order system of Cahn–Hilliard type with a supercritical nonlinearity, Adv. Differ. Equ. 7 (9) (2002) 1073–1100.
[7] G.R. Goldstein, A. Miranville, A Cahn–Hilliard–Gurtin model with dynamic boundary conditions, Discrete Contin. Dyn. Syst., Ser. S 6 (2) (2013) 387.

[8] F. Bai, C. Elliott, A. Gardiner, A. Spence, A. Stuart, The viscous Cahn–Hilliard equation. I. Computations, Nonlinearity 8 (2) (1995) 131.
[9] C.M. Elliott, A.M. Stuart, Viscous Cahn–Hilliard equation II. Analysis, J. Differ. Equ. 128 (2) (1996) 387–414.
[10] S. Gatti, M. Grasselli, V. Pata, A. Miranville, Hyperbolic relaxation of the viscous Cahn–Hilliard equation in 3-D, Math. Models Methods Appl. Sci. 15 (02) (2005) 165–198.
[11] A.N. Carvalho, T. Dlotko, Dynamics of the viscous Cahn–Hilliard equation, J. Math. Anal. Appl. 344 (2) (2008) 703–725.
[12] P.C. Fife, Models for phase separation and their mathematics, Electron. J. Differ. Equ. (2000).
[13] Q. Du, L. Ju, X. Li, Z. Qiao, Maximum bound principles for a class of semilinear parabolic equations and exponential time differencing schemes, SIAM Rev. 63 (2) (2021) 317–359.
[14] T. Tang, Z. Qiao, Efficient numerical methods for phase-field equations, Sci. Sin., Math. 50 (6) (2020) 775–794.
[15] A. Miranville, S. Zelik, Robust exponential attractors for Cahn–Hilliard type equations with singular potentials, Math. Methods Appl. Sci. 27 (5) (2004) 545–582.
[16] S. Choo, Y. Kim, Finite element scheme for the viscous Cahn–Hilliard equation with a nonconstant gradient energy coefficient, J. Appl. Math. Comput. 19 (1) (2005) 385–395.
[17] D. Wang, X. Wang, H. Jia, A second-order energy stable BDF numerical scheme for the viscous Cahn–Hilliard equation with logarithmic Flory–Huggins potential, Adv. Appl. Math. Mech. 13 (4) (2021) 867–891.
[18] L. Cherfils, M. Petcu, Energy stable numerical scheme for the viscous Cahn–Hilliard–Navier–Stokes equations with moving contact line, Numer. Methods Partial Differ. Equ. 35 (3) (2019) 1113–1133.
[19] S. Choo, S. Chung, Y. Lee, A conservative difference scheme for the viscous Cahn–Hilliard equation with a nonconstant gradient energy coefficient, Appl. Numer. Math. 51 (2–3) (2004) 207–219.
[20] J. Shin, Y. Choi, J. Kim, An unconditionally stable numerical method for the viscous Cahn–Hilliard equation, Discrete Contin. Dyn. Syst., Ser. B 19 (6) (2014) 1737.
[21] D. Li, Why large time-stepping methods for the Cahn–Hilliard equation is stable, Math. Comput. 91 (338) (2022) 2501–2515.
[22] Z. Weng, S. Zhai, X. Feng, Analysis of the operator splitting scheme for the Cahn–Hilliard equation with a viscosity term, Numer. Methods Partial Differ. Equ. 35 (6) (2019) 1949–1970.
[23] N. Zheng, X. Li, Energy stability and convergence of the scalar auxiliary variable Fourier-spectral method for the viscous Cahn–Hilliard equation, Numer. Methods Partial Differ. Equ. 36 (5) (2020) 998–1011.
[24] D. Li, Effective maximum principles for spectral methods, Ann. Appl. Math. 37 (2) (2021) 131–290.
[25] S. Zhai, Z. Weng, Y. Yang, A high order operator splitting method based on spectral deferred correction for the nonlocal viscous Cahn-Hilliard equation, J. Comput. Phys. 446 (2021) 110636.
[26] S. Injrou, M. Pierre, Stable discretizations of the Cahn–Hilliard–Gurtin equations, Discrete Contin. Dyn. Syst. 22 (4) (2008) 1065.
[27] X. Yang, J. Zhao, X. He, Linear, second order and unconditionally energy stable schemes for the viscous Cahn–Hilliard equation with hyperbolic relaxation using the invariant energy quadratization method, J. Comput. Appl. Math. 343 (2018) 80–97.
[28] H. Chen, Error estimates for the scalar auxiliary variable (SAV) schemes to the viscous Cahn–Hilliard equation with hyperbolic relaxation, J. Math. Anal. Appl. 499 (1) (2021) 125002.
[29] Y. Hao, Q. Huang, C. Wang, A third order BDF energy stable linear scheme for the no-slope-selection thin film model, Commun. Comput. Phys. 29 (3) (2021) 905–929.
[30] K. Cheng, C. Wang, S.M. Wise, Y. Wu, A third order accurate in time, BDF-type energy stable scheme for the Cahn-Hilliard equation, Numer. Math., Theory Meth. Appl. 15 (2) (2022) 279–303.
[31] D. Li, C. Quan, W. Yang, The BDF3/EP3 scheme for MBE with no slope selection is stable, J. Sci. Comput. 89 (2021) 1–24.
[32] L. Dong, C. Wang, H. Zhang, Z. Zhang, A positivity-preserving second-order BDF scheme for the Cahn–Hilliard equation with variable interfacial parameters, Commun. Comput. Phys. 28 (3) (2020) 967–998.
[33] W. Chen, C. Wang, X. Wang, S.M. Wise, Positivity-preserving, energy stable numerical schemes for the Cahn–Hilliard equation with logarithmic potential, J. Comput. Phys. X 3 (2019) 100031.
[34] T. Tang, J. Yang, Implicit-explicit scheme for the Allen–Cahn equation preserves the maximum principle, J. Comput. Math. (2016) 451–461.
[35] J. Shen, T. Tang, J. Yang, On the maximum principle preserving schemes for the generalized Allen–Cahn equation, Commun. Math. Sci. 14 (6) (2016) 1517–1534.
[36] D. Li, C. Quan, J. Xu, Stability and convergence of Strang splitting. Part I: scalar Allen–Cahn equation, J. Comput. Phys. 458 (2022) 111087.
[37] T. Hou, T. Tang, J. Yang, Numerical analysis of fully discretized Crank–Nicolson scheme for fractional-in-space Allen–Cahn equations, J. Sci. Comput. 72 (3) (2017) 1214–1231.
[38] J. Li, X. Li, L. Ju, X. Feng, Stabilized integrating factor Runge–Kutta method and unconditional preservation of maximum bound principle, SIAM J. Sci. Comput. 43 (3) (2021) A1780–A1802.
[39] H. Zhang, J. Yan, X. Qian, X. Chen, S. Song, Explicit third-order unconditionally structure-preserving schemes for conservative Allen–Cahn equations, J. Sci. Comput. 90 (2022) 1–29.
[40] H. Zhang, J. Yan, X. Qian, S. Song, Temporal high-order, unconditionally maximum-principle-preserving integrating factor multi-step methods for Allen–Cahn-type parabolic equations, Appl. Numer. Math. (2023).
[41] H. Zhang, J. Yan, X. Qian, S. Song, Numerical analysis and applications of explicit high order maximum principle preserving integrating factor Runge–Kutta schemes for Allen–Cahn equation, Appl. Numer. Math. 161 (2021) 372–390.
[42] H. Zhang, X. Qian, J. Xia, S. Song, Unconditionally maximum-principle-preserving parametric integrating factor two-step Runge-Kutta schemes for parabolic Sine-Gordon equations, CSIAM Trans. Appl. Math. 4 (1) (2023) 177–224.
[43] J. Sun, H. Zhang, X. Qian, S. Song, Up to eighth-order maximum-principle-preserving methods for the Allen–Cahn equation, Numer. Algorithms 92 (2023) 1041–1062.
[44] L. Dong, C. Wang, H. Zhang, Z. Zhang, A positivity-preserving, energy stable and convergent numerical scheme for the Cahn–Hilliard equation with a Flory–Huggins–Degennes energy, Commun. Math. Sci. 17 (4) (2019) 921–939.
[45] M. Yuan, W. Chen, C. Wang, S.M. Wise, Z. Zhang, An energy stable finite element scheme for the three-component Cahn–Hilliard-type model for macromolecular microsphere composite hydrogels, J. Sci. Comput. 87 (3) (2021) 78.
[46] L. Dong, C. Wang, S.M. Wise, Z. Zhang, A positivity-preserving, energy stable scheme for a ternary Cahn–Hilliard system with the singular interfacial parameters, J. Comput. Phys. 442 (2021) 110451.
[47] M. Yuan, W. Chen, C. Wang, S.M. Wise, Z. Zhang, A second order accurate in time, energy stable finite element scheme for the Flory–Huggins–Cahn–Hilliard equation, Adv. Appl. Math. Mech. 10 (2022).
[48] G. Beylkin, J.M. Keiser, L. Vozovoi, A new class of time discretization schemes for the solution of nonlinear PDEs, J. Comput. Phys. 147 (2) (1998) 362–387.
[49] S.M. Cox, P.C. Matthews, Exponential time differencing for stiff systems, J. Comput. Phys. 176 (2) (2002) 430–455.
[50] M. Hochbruck, A. Ostermann, Explicit exponential Runge–Kutta methods for semilinear parabolic problems, SIAM J. Numer. Anal. 43 (3) (2005) 1069–1090.

[51] M. Hochbruck, A. Ostermann, Exponential Runge–Kutta methods for parabolic problems, Appl. Numer. Math. 53 (2–4) (2005) 323–339.
[52] Q. Du, W.-x. Zhu, Stability analysis and application of the exponential time differencing schemes, J. Comput. Math. (2004) 200–209.
[53] Q. Du, W.-x. Zhu, Analysis and applications of the exponential time differencing schemes and their contour integration modifications, BIT Numer. Math. 45 (2) (2005) 307–328.
[54] K. Cheng, Z. Qiao, C. Wang, A third order exponential time differencing numerical scheme for no-slope-selection epitaxial thin film model with energy stability, J. Sci. Comput. 81 (2019) 154–185.
[55] W. Chen, W. Li, Z. Luo, C. Wang, X. Wang, A stabilized second order exponential time differencing multistep method for thin film growth model without slope selection, ESAIM, Math. Model. Numer. Anal. 54 (3) (2020) 727–750.
[56] W. Chen, W. Li, C. Wang, S. Wang, X. Wang, Energy stable higher-order linear ETD multi-step methods for gradient flows: application to thin film epitaxy, Res. Math. Sci. 7 (2020) 1–27.
[57] Q. Du, L. Ju, X. Li, Z. Qiao, Maximum principle preserving exponential time differencing schemes for the nonlocal Allen–Cahn equation, SIAM J. Numer. Anal. 57 (2) (2019) 875–898.
[58] J. Li, L. Ju, Y. Cai, X. Feng, Unconditionally maximum bound principle preserving linear schemes for the conservative Allen–Cahn equation with nonlocal constraint, J. Sci. Comput. 87 (3) (2021) 1–32.
[59] K. Jiang, L. Ju, J. Li, X. Li, Unconditionally stable exponential time differencing schemes for the mass-conserving Allen–Cahn equation with nonlocal and local effects, Numer. Methods Partial Differ. Equ. (2021).
[60] Q. Huang, K. Jiang, J. Li, Exponential time differencing schemes for the Peng-Robinson equation of state with preservation of maximum bound principle, Adv. Appl. Math. Mech. 14 (2) (2022) 494–527.
[61] H. Zhang, G. Zhang, X. Qian, S. Song, On the maximum principle and high-order, delay-free integrators for the viscous Cahn–Hilliard equation, 2022, submitted for publication.
[62] A. Novick-Cohen, R.L. Pego, Stable patterns in a viscous diffusion equation, Trans. Am. Math. Soc. 324 (1) (1991) 331–351.
[63] S.M. Wise, Unconditionally stable finite difference, nonlinear multigrid simulation of the Cahn-Hilliard-Hele-Shaw system of equations, J. Sci. Comput. 44 (1) (2010) 38–68.
[64] Z. Zhang, Z. Qiao, An adaptive time-stepping strategy for the Cahn-Hilliard equation, Commun. Comput. Phys. 11 (4) (2012) 1261–1278.
[65] S. Maset, M. Zennaro, Unconditional stability of explicit exponential Runge–Kutta methods for semi-linear ordinary differential equations, Math. Comput. 78 (266) (2009) 957–967.
[66] H. Zhang, J. Yan, X. Qian, S. Song, Up to fourth-order unconditionally structure-preserving parametric single-step methods for semilinear parabolic equations, Comput. Methods Appl. Mech. Eng. 393 (2022) 114817.
[67] A. Ostermann, M. Thalhammer, Positivity of exponential multistep methods, in: Numerical Mathematics and Advanced Applications: Proceedings of ENUMATH 2005, the 6th European Conference on Numerical Mathematics and Advanced Applications Santiago de Compostela, Spain, July 2005, Springer, 2006, pp. 564–571.
[68] A. Ostermann, M. Van Daele, Positivity of exponential Runge–Kutta methods, BIT Numer. Math. 47 (2007) 419–426.
[69] L. Ju, X. Li, Z. Qiao, H. Zhang, Energy stability and error estimates of exponential time differencing schemes for the epitaxial growth model without slope selection, Math. Comput. 87 (312) (2018) 1859–1885.
[70] Z. Fu, J. Yang, Energy-decreasing exponential time differencing Runge–Kutta methods for phase-field models, J. Comput. Phys. (2022) 110943.
[71] H. Wang, C.-W. Shu, Q. Zhang, Stability and error estimates of local discontinuous Galerkin methods with implicit-explicit time-marching for advection-diffusion problems, SIAM J. Numer. Anal. 53 (1) (2015) 206–227.
[72] D. Li, Z. Qiao, T. Tang, Characterizing the stabilization size for semi-implicit Fourier-spectral method to phase field equations, SIAM J. Numer. Anal. 54 (3) (2016) 1653–1681.
[73] J. Xu, Y. Li, S. Wu, A. Bousquet, On the stability and accuracy of partially and fully implicit schemes for phase field modeling, Comput. Methods Appl. Mech. Eng. 345 (2019) 826–853.
[74] H. Zhang, X. Qian, S. Song, Third-order accurate, large time-stepping and maximum-principle-preserving schemes for the Allen-Cahn equation, Numer. Algorithms (2023).